Universiteit Utrecht

Master Thesis

# Post-synthetic modification of zeolitic imidazolate framework-8 (ZIF-8) via cation exchange

*Author:*
Jens Schoenmakers, BSc

*Supervisors:*
Zafer Öztürk, MSc

Prof. dr. ir. Bert M. Weckhuysen

Thesis for the degree of Master of Science
In the Graduate School of Natural Sciences
Debye Institute for Nanomaterials Science
Inorganic Chemistry and Catalysis

# Abstract

Metal-Organic Frameworks (MOFs) are an interesting class of materials with high crystallinity and porosity. They are used for several potential applications, like gas separation and catalysis. There is a wide variety of MOFs known in literature, this number can be further increased by post-synthetic modification (PSM) by which the metal-ion and/or the organic linker of the framework can be modified or exchanged creating new properties for the material. A special subclass are the Zeolitic Imidazolate Frameworks (ZIFs), which have a zeolite-like topology providing extra chemical and thermal stability compared to MOFs. However, ZIFs aren't used much in catalysis due to their low activity for most reactions. The activity can be increased by modification of the framework, for example by exchanging the zinc(II)-ions with another (catalytically more active) metal(II)-ion.

In this thesis, post-synthetic modification of ZIF-8 by metal-ion exchange was studied. First ZIF-8 was synthesised in DMF, methanol and aqueous ammonia to find the most promising candidate for the post-synthetic modification. After the synthesis of ZIF-8 metal-ion exchange with manganese and cobalt was performed. With AAS and SEM-EDX the manganese and cobalt rates, after the metal-ion exchange reaction, were determined . A wide range of manganese rates was obtained, higher rates were obtained when performing the exchange reaction for longer times or at elevated temperatures. The cobalt rates found in the products were negligible. However, TEM results concluded that the metal-ions are not incorporated in the framework after the reaction but nanoparticles, which contained manganese, were observed at the surface of the particles.

# Acknowledgements

The research I've performed during my master thesis wasn't possible without the help of some people who I would like to thank. First of all I would like to thank Zafer Öztürk for offering this project to me and being my daily supervisor during my thesis. You were always around and willing to help me if I had questions. For explaining everything I needed to know for my research and learning me the analysis techniques I had to use. I would like to thank Bert Weckhuysen and Pieter Bruijnincx for the opportunity to perform my master thesis at this group.

I also would like to thank the following people who helped me with different analysis techniques. Marjan Versluijs-Helder (XRD, SEM and SEM-EDX), Fouad Soulimani (FTIR), Joe Steward and Mies van Steenbergen (TGA), Hans Meeldijk (TEM and TEM-EDX), Rogier Brand and Stephan Jonker (AAS) and Nazila Masoud, Ying Wei and Pasi Paalanen ($N_2$-physisorption). For being a great neighbour during my thesis, I would like to thank Jochem Wijten. We've had a lot of useful discussions about our work and also had a lot of fun during the research. Last but not least I would like to thank the whole Inorganic Chemistry and Catalysis group for the great time I've had. I have enjoyed the time I have spent during my research in this group, thank you all!

# Contents

# List of Figures

# List of Tables

# List of Abbreviations

| | |
|---|---|
| AAS | Atomic Absorption Spectroscopy |
| ATR | Attenuated Total Reflectance |
| bdc | Benzene Dicarboxylate |
| DMF | Dimethylformamide |
| EDX | Energy Dispersive X-ray Spectroscopy |
| FTIR | Fourier Transform Infrared Spectroscopy |
| HAADF | High-Angle Annular Dark Field |
| HMeIm | 2-methylimidazole |
| MOF | Metal-Organic Framework |
| PCP | Porous Coordinated Polymer |
| PSD | Post-Synthetic Deprotection |
| PSE | Post-Synthetic Exchange |
| PSM | Post-Synthetic Modification |
| SALE | Solvent-Assisted Linker Exchange |
| SDC | *trans*-4,4'-Stilbene Dicarboxylate |
| SEM | Scanning Electron Microscopy |
| TEM | Transmission Electron Microscopy |
| TGA | Thermogravimetric Analysis |
| XRD | X-Ray Diffraction |
| ZIF | Zeolitic-Imidazolate Framework |

# 1 Introduction

Porous materials are an important class of materials used for many applications such as gas storage, separation and catalysis. Worldwide the economic value of porous materials is estimated up to 350 billion dollars per year [1,2]. Porous materials possess a high surface area per gram compared to non-porous materials which makes them more promising for applications that need surfaces to interact, such as gas storage, drug delivery and catalysis [3,4]. A well known class of porous materials are zeolites which are crystalline porous aluminosilicates constructed by $TO_4$ building blocks where T mostly stands for $Si^{4+}$ or $Al^{3+}$ cations coordinated by $O^{2-}$ anions [5]. To date 225 structures are registered by the International Zeolite Association (IZA) [6]. Two of the most known zeolites are zeolite Y and ZSM-5, both zeolites are used as catalysts in the petrochemical industry [7,8].

A breakthrough in porous materials was the discovery of Porous Coordination Polymers (PCPs), which often possess permanent porosity, even without guest molecules inside the pores [10]. PCPs were mentioned for the first time in 1964 by Bailar et al. [9,11] and this created a third class of porous materials. Figure 1.1 shows three different classes of porous materials, which are carbon-based materials (e.g. activated carbon), inorganic materials (e.g. zeolites) and coordinated polymers (e.g. PCPs) [9].

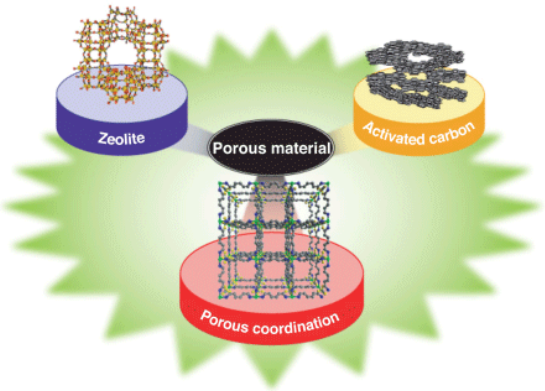


Figure 1.1: Different classes of porous materials [9].

As mentioned before, in industry mostly zeolites are used due to their high thermal and chemical stability compared to other porous materials [12]. With 225 structures known, the number of available zeolites is limited [6,10], therefore research is performed to find a material which is porous and has a thermal and chemical stability comparable to zeolites, but has a larger versatility to obtain materials with a larger range of applications. With the discovery of PCPs a lot of research has focused on these materials [13], which are built up by metal-ions or metal clusters bridged by organic molecules. This gives rise to a great versatility of PCPs that can be created. Since Yaghi et al. mentioned it for the first time, PCPs are mostly called as Metal-Organic Frameworks (MOFs) [14]. This publication gave a boost to the research on MOFs, which is an interesting class of materials due to their high crystallinity and porosity. This resulted in high surface areas (up to

7000 $m^2g^{-1}$) and pore volumes (up to 4.4 $cm^3g^{-1}$)[15] compared to other (porous) materials. This increase in research is clearly shown by the amount of articles published about MOFs over years. Figure 1.2 shows the amount of documents registered by Scopus; a huge increase in documents can be seen over years.

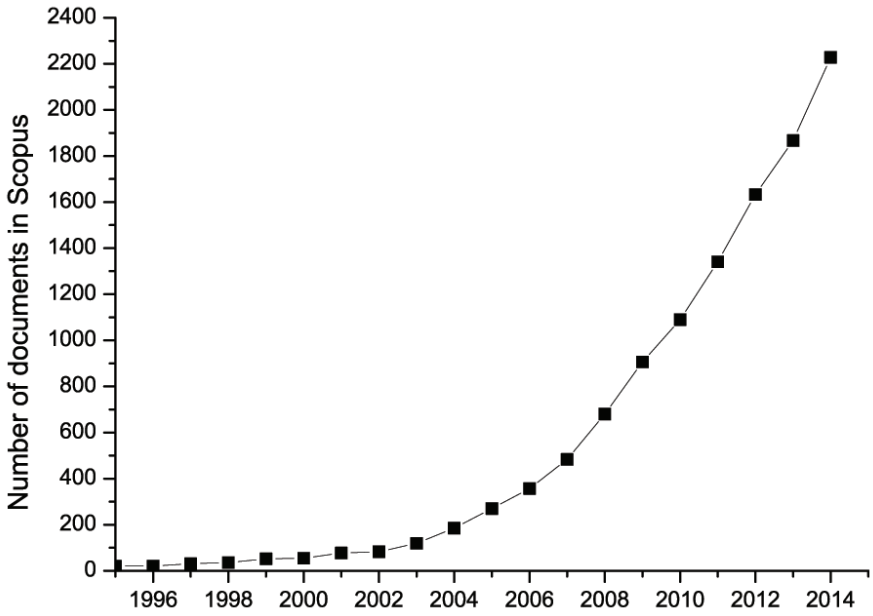


Figure 1.2: Amount of documents registered in Scopus when searched with the keywords "metal organic frameworks" sorted by year (09-04-2015).

This increasing interest in MOFs is due to the great versatility of these materials; which are constructed out of metal-ions or metal clusters bridged by organic linkers. Almost every (d-block transition) metal can be used as metal node, which gives a wide variety. For the bridging linkers a lot of organic molecules can be used, usually multidentate organic linkers such as amines, carboxylates, imidazolates, phosphates, pyridines and sulphates are used[12,16]. By using different synthesis parameters, the topology of MOFs can also be altered to create materials with the same molecular formula but with different structures[17]. The combination of those three gives a huge variety of MOFs that can be synthesised, examples of this possible variety are shown in Figure 1.3[17].

MOFs can be used for a wide range of applications like gas storage[12,18,19], separation[12,19,20], sensing[18,20,21] and catalysis[10,12,19,20,22]. One of the subclasses of MOFs are the Zeolitic Imidazolate Frameworks (ZIFs)[23,24].

ZIFs are an important subclass of MOFs; they are composed of metal-ions, mostly $Zn^{2+}$ and $Co^{2+}$, bridged by imidazolate derivatives[1]. The metal-ions are tetrahedrally coordinated by the nitrogen atoms in the 1,3-positions of imidazole. As shown in Figure 1.4 the M-Im-M angle (M = metal-ion, Im = imidazolate)

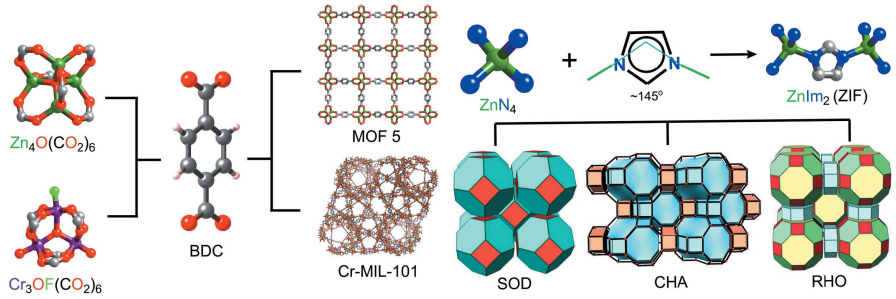


Figure 1.3: Example of the diversity of MOFs with different metal-ions, organic linkers or structures[17].

in ZIFs is similar to the Si-O-Si angle in zeolites (145°)[1,2,25]. This similar angle results from ZIFs having a zeolite-like topology which provides extra chemical and thermal stability compared to most MOFs[1,26,27]. Different structures can be obtained by varying the linkers, even structures that aren't known for zeolites[20]. Many imidazole derivatives can be used for the synthesis of ZIFs. In Figure 1.5 examples are shown of the different, functionalised, linkers that can be used[28].

Due to their high chemical and thermal stability compared to other MOFs, ZIFs became an interesting material with many possible applications[19,21,25]. ZIFs have advantages of both MOFs and zeolites: they combine the porosity, crystallinity and the chemical versatility of MOFs with the chemical and thermal stability of zeolites[19], however the chemical and thermal stability of ZIFs is lower compared to zeolites[8,29]. Because of its facile synthesis and potential applications in gas storage/separation and catalysis, ZIF-8 is one of the most studied ZIF materials[24,28].

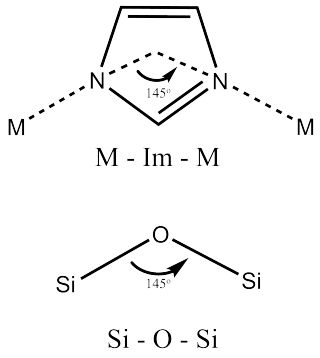


Figure 1.4: The M-Im-M angle in ZIFs is similar to the Si-O-Si angle in zeolites (145°), which provides extra stability to the framework compared to MOFs[1].

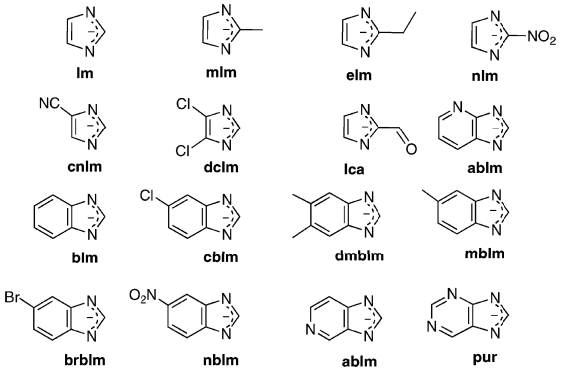


Figure 1.5: Example of the different imidazolate linkers that are possible for the synthesis of ZIFs[28].

A consequence of the extra stability of ZIFs compared to MOFs is the lower

activity of these materials for catalysis[30], this might be due to the saturated metal sites in ZIFs[31]. The catalytic activity of ZIFs can be increased by use of post-synthetic modification (PSM), which is a powerful tool to design materials for a specific application[28]. PSM can be performed on both organic linkers and metal nodes of the ZIFs, obtaining a framework with desired properties. The most used modification methods performed on ZIFs (and MOFs) are solvent-assisted linker exchange (SALE) and metal-ion exchange[32–34].

This thesis is focussed on the post-synthetic modification of ZIF-8 by metal-ion exchange to obtain a framework which is catalytically more active than the parent ZIF-8. Cation exchange has been performed to replace the $Zn^{2+}$-ions by different metal-ions ($Cu^{2+}$, $Co^{2+}$ and $Mn^{2+}$) without disturbing the crystal structure of the framework. First ZIF-8 was synthesised using three different methods to find the most promising candidate for the exchange reaction. When this has been done, metal-ion exchange was performed on the parent material using different parameters to see what gives the best results.

# 2 Theory

## 2.1 Metal-Organic Frameworks

MOFs are formed by the self-assembly of metal-ions, which act as coordination centre, bridged by organic ligands to form crystalline solids[22]. Due to the absence of non-accessible volume in MOFs, they have, on weight-specific basis, the highest porosity and surface area[22]. This leads to a high density of fully exposed active sites per volume.

The topology of MOFs can be influenced by several parameters. One factor is the preferred geometry of the metal-ions and linkers used for the synthesis[35]. Another important factor is the synthesis medium, which can interact with the framework during the synthesis. The solvent can play different roles during the synthesis of MOFs, it can act as ligand, guest, both as ligand and guest and as a structure-directing agent[36]. The solvent can also affect the MOFs crystallinity, for instance, Bustamante et al. investigated the crystallinity of ZIF-8 synthesised in different alcohols. They found that the highest crystallinity of ZIF-8 was obtained in methanol and n-octanol. The lowest crystallinity was observed when 2-butanol was used for the synthesis[37].

One of the driving forces in the MOFs research is their potential use for many applications[38], as they can bridge the gap between zeolites and enzymes[10] and also can combine the benefits of both heterogeneous and homogeneous catalysis[12]. Nine-out-of-ten chemical processes make use of heterogeneous catalysts[22]. As mentioned in the introduction, MOFs can be tuned since different metal-ions and organic linkers can be used for the synthesis. Also combinations of different metal-ions or linkers can be used, resulting in different functionalities within the framework[39]. This makes it possible to design the MOFs with desired properties for different applications[40]. The variety of MOFs that can be synthesised using different linkers was shown by Eddaoudi et al. They synthesised a set of MOFs based on MOF-5 but with the presence of different functional groups (such as halogens, hydroxyl and amino groups) or by changing the size of the organic linker[41].

MOFs are used in catalysis in three different ways[12].

- The active site for catalysis is part of the framework
- An catalytically active specie is located in the pores of the MOFs, bound by non-covalent interactions
- The active site is introduced in the framework by post-synthetic modification

The oldest reports about MOFs in catalysis used MOFs in which the active site is an intrinsic part of the framework[12]. Examples for those reactions are the cyanosilylation of aldehydes[42] and the Friedel-Crafts benzylation[43]. This

method is interesting as the MOFs can be used directly after the synthesis procedure without any extra step needed. However, since the active site is part of the framework, it also contributes in the frameworks stability. One can imagine that the stability of the frameworks decreases when it is used for catalysis, this can result in changes in, for example, crystal structure. This can lead to deactivation of the catalyst, therefore having the active site as an intrinsic part of the framework has some disadvantages.

This can be avoided when the active site is not part of the framework, for example when it is located in the pores of the MOFs by non-covalent interactions. In this case MOFs are used as supporting materials, like zeolites, providing a porous structure with a surface on which catalytic active species (for example metal nanoparticles) can be placed. An example of MOFs used as support is the oxidation of a-pinene by polyoxotungstate nanoparticles placed in the cages of MIL-101[44].

The versatility of MOFs is a great property in the use of MOFs for different applications. Additional to this great property, the versatility of MOFs can be increased by modification of the frameworks. This method gives the possibility to create materials which are designed for a special application by combining interesting properties of both metal sites and organic linkers. Due to the great tunability of MOFs they might be useful for shape selective catalysis, as reported by Jones et al.[45]. They showed the difference between a reaction performed under homogeneous and heterogeneous conditions. For the homogeneous reaction they treated *trans*-4,4'-stilbene dicarboxylate (SDC) with $Br_2$ in $CH_2Cl_2$, resulting in a 4:1 ratio of the *meso*- to *rac*-isomers. When the heterogeneous reaction was performed SDC was first used to synthesise a MOF with the formula $Zn_4O(SDC)_3$, which then was treated with $Br_2$. With this reaction only the *meso*-isomer was obtained. This difference is caused by the immobilisation of the SDC linker as part of the framework which inhibits the rotation of the carbon-carbon bond.

However, a disadvantage of MOFs for catalysis is their lower thermal (300-400℃ for carboxylate and imidazolate-based MOFs), hydrothermal and chemical stability compared to zeolites[10,46]. This makes them less suitable for reactions using high temperatures or pressures, but they might be useful for the synthesis of fine chemicals[12]. To solve the problem with the lower stability, research has been performed to find MOFs which have a higher chemical and thermal stability, with a breakthrough when the zeolitic imidazolate frameworks were discovered; this subclass of MOFs will be discussed in the next section.

### 2.1.1 Zeolitic Imidazolate Frameworks

Zeolitic Imidazolate Frameworks (ZIFs) are a subclass of MOFs which have a zeolite-like topology. They are composed of metal-ions, mostly $Zn^{2+}$ or $Co^{2+}$, and

imidazolate derivatives as organic linkers[47]. The type of imidazolate and the solvent used in the synthesis of ZIFs have a great influence on the structure that is obtained[28]. By use of large imidazolate derivatives new topologies can be obtained due to steric hindrance[1]. The imidazolate linker can also be functionalised to achieve ZIFs with desired functionality for a specific application.

Because of its easy and reproducible synthesis, ZIF-8 is one of the most studied ZIFs[28]. ZIF-8 is composed of zinc(II) ions and 2-methylimidazolate (MeIm) which results in the sodalite topology formed by four- and six-member rings of $ZnN_4$ clusters with internal cavities of 1.16 nm connected by 0.34 nm windows[2]. ZIF-8 has a high chemical and thermal stability compared to other MOFs. It can be boiled in different solvents without losing its crystallinity and porosity[1] and is stable up to 550°C[2]. ZIF-8 is stable in water because of its hydrophobic framework, which is due to the HMeIm linkers[19].

HMeIm has an influence on the formation of ZIF-8. Imidazole has $pK_{a1}$=7.1 and $pK_{a2}$=14.2 in methanol, which makes it possible to be in both neutral and deprotonated form during the synthesis[48]. During the synthesis HMeIm acts both as linker (when it is deprotonated) and as stabilising agent (in its neutral form). The fraction of HMeIm used for the synthesis influences the average crystallite size, increasing the HMeIm fraction leads to a decrease in average crystallite size[48,49]. This might come due to the increasing amount of deprotonated molecules for coordination with $Zn^{2+}$, this causes a higher nucleation rate which results in a smaller crystallite size. To obtain nanosized ZIF-8 crystals, a fast nucleation and slow crystal growth is needed[26]. The crystal size also depends on the synthesis time, with increasing time the crystal size increases due to a longer growth stage during the synthesis[50].

Another parameter on the crystal size is MeOH/$Zn^{2+}$ molar ratio, this also influences the rate of crystallisation. Keser Demir et al. discovered that an excess amount of methanol leads to a decrease in particle size and rate of crystallisation, as shown in Figure 2.1 A[26]. When the MeOH fraction is increased the concentrations of $Zn^{2+}$ and HMeIm decrease which results in a relative increase of the number of nuclei formed leading to a smaller crystallite size.

The synthesis time for ZIF-8 can be shortened by adding a base to the synthesis mixture. The base deprotonates the imidazole linker for a faster nucleation which increases the reaction rate through which higher yields are obtained[51]. The shape-evolution of ZIF-8 over time with a base added is shown over time in Figure 2.1 B[47], in the figure can be seen that:

- After 2 minutes, slightly round particles with hexagonal plate contour are formed on which small nanoparticles were deposited.
- After 5-10 minutes, the surface of the particles change gradually from rough to smooth with less defects. The amount of small particles visible on the

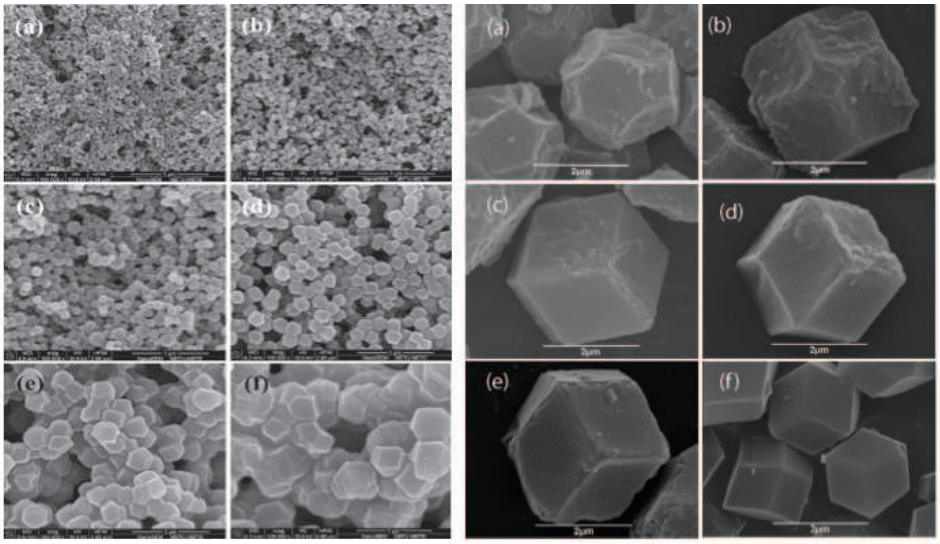


Figure 2.1: Influences of (A) time on the ZIF-8 growth and (B) the MeOH : $Zn^{2+}$; In figure A the influence of the MeOH : $Zn^{2+}$ ratio on the ZIF-8 crystal size is shown with SEM images; MeOH : $Zn^{2+}$ molar ratio of: (a) 1043; (b) 695; (c) 528; (d)348; (e) 174; (f) 87[26]. Figure B shows the evolution of ZIF-8 particles over time during the synthesis: Reaction performed in aqueous ammonia, the molar ratio $Zn^{2+}$:MeIm:$NH_3 \cdot H_2O$ is 1:2:400. (a) 2 min; (b) 5 min; (c) 10 min; (d) 1 h; (e) 6 h and (f) 24 h[47].

surface has decreased.

- After 24 hour, rhombic dodecahedron shaped particles are shown with a very smooth surface without defects. The particles are 2 µm in size.

It is likely that with increasing reaction time the supersaturation of the solution gradually decreases, this leads to a decrease of the nucleation rate. This results in an increase of the crystal growth[47]. The size and shape of ZIF-8 synthesised in methanol can also be tuned by use of modulating agents or stabilizers, for example bridging agents or surfactants[52,53].

## 2.2 Synthesis methods

For the synthesis of MOFs several parameters has to be taken into account. The obtained structure is dependent on the reaction conditions used during the synthesis, like reagents, solvent and temperature[54,55]. The preferred coordination of the metal-ions used during the synthesis in combination with the linkers determine the obtained geometry of MOFs. For example, ligand field theory says that zinc(II)

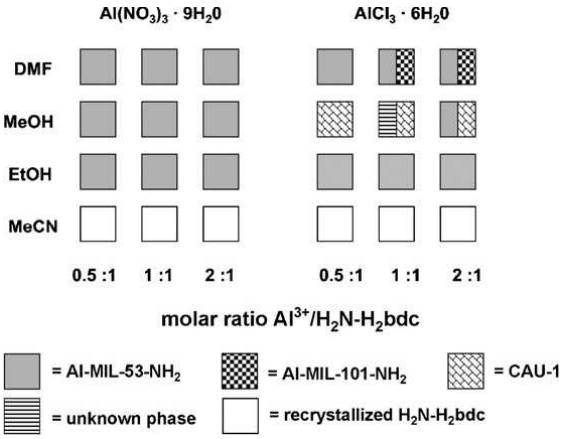


Figure 2.2: Influence of different solvents and molar ratios of the reagents on the structure formed. Two $Al^{3+}$ precursors are used in the reaction with aminotereph-talic acid ($H_2N-H_2bdc$) obtaining different topologies in different solvents [54].

prefers the tetrahedral geometry while manganese(II) prefers the octahedral geometry when combined with 2-methylimidazolate [35].

Solvents have a big influence on the MOFs synthesis, as shown in Figure 2.2 different structures can be formed by using different solvents [54,56]. The solvent can act as ligand during the synthesis, coordinating to the metal-ion leading to a structure. The pores of the MOFs are always filled with solvent during the synthesis, which act as space-filling molecule. MOFs can carry 50-150 wt% of solvent in the pores [22], upon removal of the solvent from the pores, in many cases the structure of the MOFs collapses [4,57]. To prevent the collapse of the structure, the removal of the solvent from the pores has to be performed carefully. First the drying of the MOFs has to be done under gentle conditions to remove most of the solvent, after which activation can be performed at higher temperatures to completely evacuate the pores.

Temperature can affect the synthesis of MOFs in different ways. The solubility of the organic linker depends on the temperature used during the synthesis, higher temperatures results in a higher solubility of the linker. Temperature can also provide the energy required for the reaction to occur and can increase the reaction rate [58]. Different synthesis temperatures can result in different structures for MOFs [55,59].

### 2.2.1 Solvothermal synthesis

A definition for solvothermal reactions is given in the paper of Stock et al.: "Reactions taking place in closed vessels under autogeneous pressure above the boiling point of the solvent" [13,28]. The driving force for this method is the reaction tem-

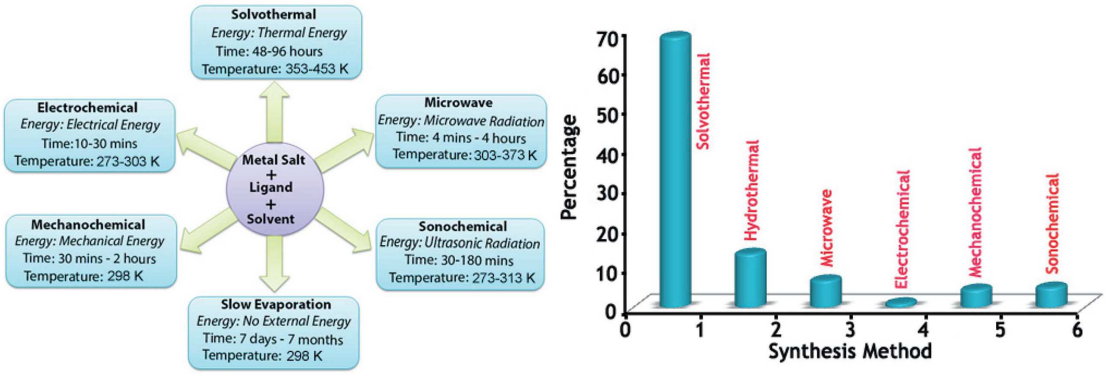


Figure 2.3: In the left picture different solvent-based synthesis methods are shown with their driving forces and the common synthesis conditions used for the method. In the right picture the usage of the different methods in percentages is shown; most times the solvothermal method is used [17].

perature. As shown in Figure 2.3, the solvothermal method is the most used method for MOFs syntheses [17], this might be due to the simplicity of the method. The method is schematically shown in Figure 2.4. Usually the reagents are first dissolved, the solutions are mixed and placed in a closed vessel. The vessel is placed in an oven at elevated temperature, which doesn't have to be above the boiling pressure of the solvent, for 24-48h. During this time the MOFs are formed as solid crystals by self-assembly which can be collected by filtration. The product is washed several times to remove any reagent left and finally dried in an oven to remove the solvent and evacuate the pores [2,60].

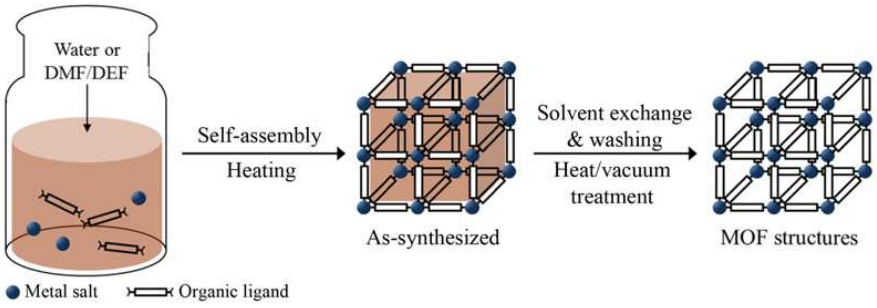


Figure 2.4: Schematic drawing of the solvothermal synthesis method [61], the reagents are dissolved after which they self-assemble under heating to form MOFs. After the synthesis the products is washed and dried to obtain the MOFs with empty pores.

As a solvent mostly dimethylformamide (DMF) is used, however, due to its tox-

icity and environmental unfriendly nature, research is performed to find protocols using other solvents. Many protocols using methanol as solvent are developed; beside the advantage that methanol is less toxic than DMF, it also has the advantage that this synthesis can be performed at room temperature[24].

### 2.2.2 Hydrothermal synthesis

Since organic solvents are expensive, flammable and not environmental friendly, research has been performed to develop methods which use less (or even better completely avoid) organic solvents[62]. For this reason, synthesis methods based on aqueous systems are preferable since they are environmental friendly compared to methods based on organic solvents. For ZIF-8 synthesis, Pan et al. were the first who found a method to synthesise ZIF-8 using an aqueous system at room temperature[63]. But they had an other problem with their synthesis; they used a $Zn^{2+}$ : HMeIm molar ratio of 1:70, which means a lot of HMeIm doesn't react and is spilled using this method (to compare, the $Zn^{2+}$ : HMeIm molar ratio in ZIF-8 is 1 : 2). To lower the excess amount of linker needed, auxiliary agents can be used to help the formation of the desired product. Auxiliary agents, for example triethylamine (TEA) or concentrated ammonia can assist with the deprotonation of the imidazole and initiate the formation of ZIF-8[64]. Yao et al. reported a $Zn^{2+}$ : HMeIm : $NH_4{}^+$ : $H_2O$ molar ratio of 1 : 2 : 16 : 547, which means that they could synthesise ZIF-8 using a stoichiometric molar ratio for the reaction[65].

### 2.2.3 Other synthesis methods

**Microwave synthesis**
The microwave synthesis method is based on the interaction of electromagnetic waves with mobile electric charges (e.g. polar solvent molecules/ions in solution). When using the right frequency, collisions between molecules will take place which will lead to an increase in kinetic energy resulting in an increase in temperature[61]. Microwave heating is an efficient way of heating, it has the possibilities of using heating ramps and homogeneous heating, however the solvent and energy input have to be chosen carefully[13]. An advantage of microwave-assisted method over the solvothermal method is the increased reaction rate still with the possibility to control the size of the particles, however most times the crystallinity of the obtained particles is worse compared to the particles obtained with conventional heating[13,66].

**Electrochemical synthesis**
Electrochemical synthesis relies on redox chemistry between a solid metal and a solution of the organic linker. The advantage of electrochemical methods is that

they don't need a metal salt, the metal-ions are supplied by anionic dissolution to a solution of the linker with the production of $H_2$ [13,28,61]. Other advantages of this method is the shorter reaction time and lower temperatures needed compared to the solvothermal method [28,67]. However, since most organic linkers are hardly soluble in water, organic solvents are needed in which electrochemistry is less known than in aqueous systems [67].

**Mechanochemical synthesis**
Research has been performed to find a synthesis method that doesn't need a solvent. This is an advantage since organic solvents can be avoided making it an possible green synthesis method [20]. It also has the advantage that the product has empty pores which avoids the problem of collapsing the structure while removing the solvent in the pores [68]. One solvent-free method is the mechanochemical synthesis method, the solid reagents are mixed and ground mechanically forming the desired MOFs [66]. For the grinding mostly a ball mill is used which is a drum with balls inside that is rotated, the balls fall onto the solids crushing it to a fine powder [69].

## 2.3 Post-Synthetic Modification (PSM)

Post-synthetic modification (PSM) is a way to tune a material after the synthesis, for example by adding functional groups to the linker or by changing the metal-ions in the material, without changing its topology [70]. Due to their great chemical variety PSM is performed many times for MOFs to develop crystalline porous materials with desired properties. This is done by incorporation of a functionality group on the organic linkers or by changing the metal-ions. In some cases the direct synthesis of MOFs with desired functionality is hard to perform [71]. This can have several reasons such as limited linker solubility, chemical and/or thermal stability, the preferred geometry of the metal-ion/organic linker or the desired functional group can preclude the formation of the desired structure [35,72]. Also undesired reactions can occur between the functionalised linker and the metal-ion leading to undesired products. For example interactions between metal-ion and linker can lead to the formation of different structures, for instance amorphous products can be formed [72]. When self-assembly doesn't give the desired MOFs with functionalised linkers, post-synthetic modification (PSM) can help designing the desired MOFs [10,72,73] as shown in Figure 2.7 [73].

For gas storage and catalysis, a requirement for MOFs is that they have accessible and coordinatively unsaturated metal sites to bind gases/substrates. Those metal sites are normally hard to obtain directly using solvothermal synthesis. With PSM the unsaturated metal sites can be created in the framework [74]. There are different approaches to modify the metal sites or the linkers in MOFs:

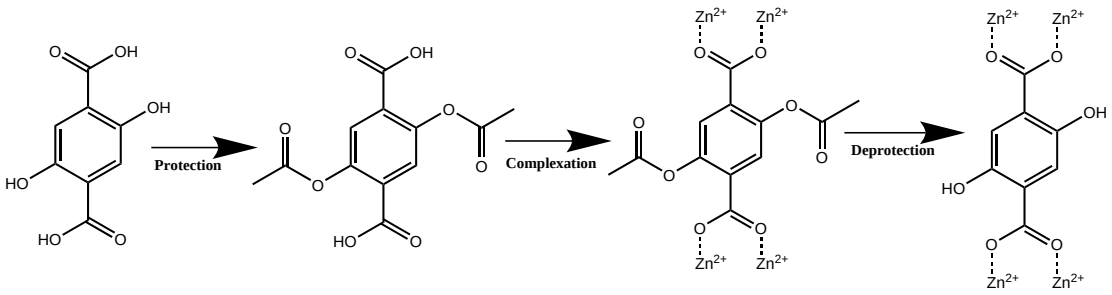


Figure 2.5: The principle of post-synthetic deprotection: First the functional group is protected by introducing a protecting group (protection). Second the linker reacts with the metal-ion to form the MOFs (complexation). Finally the protecting group is removed to obtain the framework with functionalised linkers (deprotection) [78].

**Covalent post-synthetic modification**

When modifying MOFs after the synthesis by replacing a functional group on the linker, it is called covalent post-synthetic modification (often called post-synthetic modification). As the name suggests, the framework is modified by a functional group that is covalently attached [75]. This is mostly performed with functionalisation of the organic linker by addition or substitution of a functional group [76]. But functionalisation can also be performed by the addition of a dative bond to the framework [77].

**Post-synthetic deprotection (PSD)**

Some kinds functional groups on linkers prevent the formation of the desired MOFs, they can, for example, coordinate to the metal-ions. To prevent this unwanted coordination the functional groups can be protected, when the MOFs are synthesised post-synthetic deprotection can be performed to remove the protective group the framework. An example of PSD is shown in Figure 2.5 performed by Yamada et al. [78]. First the alcohol groups of the organic linker are protected acetyl groups with the formation of ester bonds, then the MOFs are formed after which the protective acetyl groups are removed.

**Post-synthetic exchange (PSE)**

Post-synthetic exchange (PSE) is used to exchange the linker or the metal-ions in MOFs. With this method topologies can be created with a composition of metal-ions and linkers which can't be synthesised directly. PSE has become a facile technique to modify MOFs under mild conditions [74]. This makes it possible to perform PSE on a wide range of MOFs, despite their relative low stability. As shown in Figure 2.6, PSE can be performed in two ways, it can be a reaction

between two solids exchanging their linkers/metal-ions or a reaction between a solid and a solution of the linker/metal-ion[79]. Two often used PSE methods will be discussed in more detail in the sections 2.3.1 and 2.3.2.

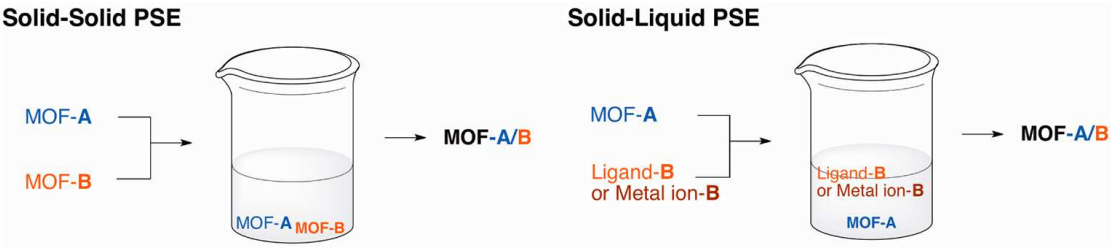


Figure 2.6: Two ways to perform post-synthetic exchange, solid-solid and solid-liquid[79].

Beside the possibility to change the linker/metal-ion, functionalising the linker with different groups can modulate the cavity size without changing the structure of the framework[12]. PSM is performed after the synthesis of the framework. This make it possible to create materials with a specific structure and desired functional groups optimising it for different applications[79]. Other crystalline materials, such as zeolites, don't have the accessible chemical functionality and the size of open space to have many possibilities for post-synthetic functionalisation[12]. This makes other porous crystalline materials less suitable for post-synthetic modification compared to MOFs[79]. Amorphous mesoporous structures lack the perfect homogeneous surface for controlled modification.

In Figure 2.7 the principle of post-synthetic modification is shown. When it isn't possible to first modify the linker and then synthesise the functionalised MOFs, the original MOFs has to be synthesised first after which the framework can be modified by exchanging the linkers with the desired functional group to obtain the desired MOFs.

PSM has some advantages, it is a heterogeneous process which makes isolation of the product easy by filtration. Another advantage of the heterogeneous reaction is that only the metal-ion or organic linker has to be dissolved. This prevents any problems with dissolving two different chemicals, for example a polar and an apolar reagent, with the possibility that they don't dissolve in the same solvent. The modification of MOFs can be repeated multiple times, which gives the possibility to incorporate different functional groups in the framework resulting in different functionalities within a material[73].

Although PSM can be performed under more different conditions compared to the solvothermal synthesis, it still has some requirements. So must the MOFs contain a functional group or metal-ion that can be modified or replaced. Also must the MOFs be stable under the reaction conditions (e.g. temperature and solvents)

used for the modification and shouldn't any by-products be formed during the reaction (e.g. acids) which can destroy the framework [73].

The most used method for post-synthetic modification is performed by placing the MOFs in a solution of the desired linker or metal-ion, at elevated temperature if necessary, for some time (from days to weeks). There will be an equilibrium between the linkers/metal-ions in the framework and in the solution, by which they will exchange without loss of crystallinity or porosity of the material [79,80].

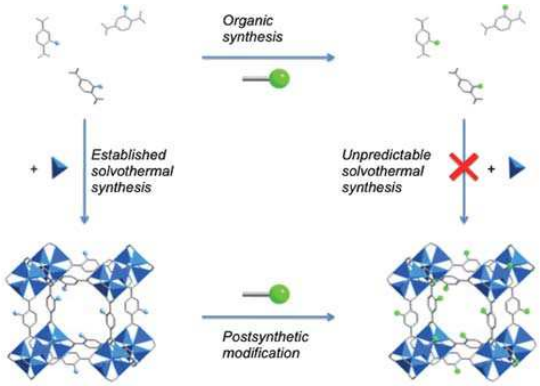


Figure 2.7: Post-synthetic modification makes it possible to form MOFs which can't be synthesised directly by conventional synthesis techniques. First the MOFs has to be synthesised after which the desired functionality can be added to the linker [73].

### 2.3.1 Solvent-assisted linker exchange (SALE)

Solvent-assisted linker exchange (SALE, in literature also called bridging linker replacement [81] and post-synthetic ligand exchange [82]) is, as the name presumes, the exchange of the linker of MOFs by another organic linker assisted by a solvent [72]. It is an easy method to exchange linkers in MOFs for functionalised linkers by a heterogeneous reaction in which the MOFs are submerged in a concentrated solution of the desired linker [23,33]. This results in a "new" framework with the same topology and metal-ions as the parent material but with functionalised linkers which leads to new properties for the material. It has to be taken into account that the size of the linkers influence the exchange rate of SALE; smaller linkers can fit into the pores of the MOFs which makes it easier for the exchange. SALE with larger linkers is more difficult to perform, but Karagiaridi et al. [33] and Li et al. [83] were able to perform linker exchange by larger linkers.

The process of linker exchange is reversible, it is possible to first exchange a linker by a functionalised linker and then exchange the functionalised linker with the original linker [72]. Gross et al. calculated that the Gibbs free energy for the linker exchange reaction in MOF-5, in which benzene dicarboxylate (bdc) was exchanged for 2-bromobenzene dicarboxylate (Br-bdc), was approximately zero [84]. From this result one can conclude that the exchange reaction is an equilibrium between the linkers in the framework and the linkers in the solution.

A parameter that influence the rate of the exchange reaction is the size of the crystals; Takaishi et al. found that smaller crystal sizes lead to a faster rate

of exchange compared to larger crystals[32]. This suggests that diffusion plays a significant role in the exchange process for reaching the equilibrium. The solvent also plays an important role in the exchange rate; a solvent is needed in which the linker dissolves and which makes it possible to diffuse into the pores of the MOFs[72]. However, until now the exact role of the solvent still is unclear; Brozek et al. performed a solvent study from which they concluded that the polarity and the coordinating ability of the solvent plays a role for the exchange reaction[85].

### 2.3.2 Metal-ion exchange

Besides the exchange of the linkers, the metal-ion/nodes can also be modified in MOFs; this can be performed by impregnation of metal particles in the framework[46] or by exchanging the metal-ions[23]. This is called metal-ion exchange (shown in Figure 2.8), in literature also called transmetalation[72] or metal metathesis[80]. The metal-ions in the framework are replaced by other metal-ions to obtain

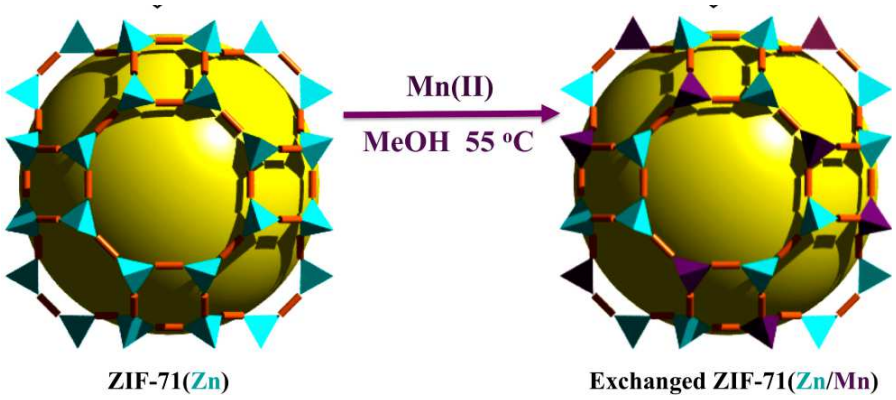


Figure 2.8: Metal-ion exchange in ZIF-71; on the left ZIF-71 ($Zn^{2+}$ with 4,5-dichloroimidazolate) is shown, upon soaking in a solution of a manganese(II) precursor at 55°C $Zn^{2+}$ ions are partially exchanged with $Mn^{2+}$ ions to obtain ZIF-71(Zn/Mn)[23].

better properties for an application[73]. The reaction is performed by submerging the MOFs in a solution of a metal precursor (often a metal salt)[72,86]. The different metals that can be placed in the framework influences the stability of the framework, this framework stability follows the trend of the Irving-Williams series for transition metal complexes[87]. The Irving-Williams series[88] for transition metal complexes is:

$$Ba^{2+} < Sr^{2+} < Ca^{2+} < Mg^{2+} < Mn^{2+} < Fe^{2+} < Co^{2+} < Ni^{2+} < Cu^{2+} > Zn^{2+}$$

The process of metal-ion exchange is reversible[80,84], however the reverse reaction might proceed slower due to weaker interactions of the metal-ion with the

linker[87].The replacement of the metal-ions in MOFs can be both partial and complete, this process can be influenced by several parameters. The concentration of the metal-ion in solution influences the exchange rate; if the concentration is higher the exchange rate will also increase. When the metal concentration is too low, the metal-ions get adsorbed to the surface of the framework[87], increasing the concentration of the metal-ion shifts the equilibrium to the exchange of the metal-ions instead of the adsorption. An excess of the metal-ions in solution, compared to the metal-ions in the framework, is required to obtain fully exchanged frameworks[87,89]. Obviously the exchange rate depends on the time for the exchange reaction; the longer the reaction time, the higher the exchange rate until equilibrium has been reached.

Another great influence on the exchange is the radius and preferred geometry of the metal-ions[87]; if the exchanging metal-ion has a radius which is different from the original metal-ion or if the preferred geometry is different (for example a preferred octahedral geometry instead of a preferred tetrahedral geometry) the structure might be destroyed by the exchange. As mentioned before, the stability of the framework has to be taken into account when performing metal-ion exchange; the framework has to be stable under conditions used for the exchange reaction, otherwise the framework might be destroyed[87].

## 2.4 Analysis methods

During this research different analysis techniques were used to characterise the materials.

### 2.4.1 X-Ray Diffraction

With X-Ray Diffraction (XRD) the crystallinity of a material can be determined; a sample is irradiated by X-rays of a known wavelength. Depending on the angle of irradiation and the lattice spacing of the material, the X-rays will be scattered by the material. This can be described by Bragg's Law:

$$2d \sin\theta = n\lambda$$

In this formula, d describes the lattice spacing inside the material; $\theta$ is the angle between the incident X-ray beam and the lattice planes; n is an integer and $\lambda$ is the wavelength of the incident X-rays.

**Measurements**
For the X-ray diffraction measurements a D2 Phaser from Bruker was used. The samples were ground obtaining fine powders before the measurements. The powder was placed on the sample holder taking into account that approximately the

same amount of sample was used for every measurement. The diffractograms were measured from $2\theta$ = 5-50°, with a increment of 0.024° and an integration time of 0.1 seconds. The measurements were performed at room temperature using a Co K$\alpha_{1,2}$ radiation source ($\lambda$ = 1.9026 Å) while the sample was rotated with 15 rotations per minute. The high temperature X-ray diffraction measurement was performed with a AXS D8 Advance powder X-ray diffractometer from Bruker. The same parameters, as for the normal XRD measurements, were used for this measurement under inert conditions.

### 2.4.2 Infrared spectroscopy

To characterise the different chemical bonds in a material infrared spectroscopy (IR) can be used. IR is a non-destructive spectroscopy technique which uses light to measure different vibrations in a material. A sample is irradiated with light in the infrared range, light of a specific wavelength is absorbed by a molecule which changes its vibrational motion. This absorption can be detected by looking at the difference between the background scan, in which a spectrum is measured without a sample, and the spectrum measured with the sample.

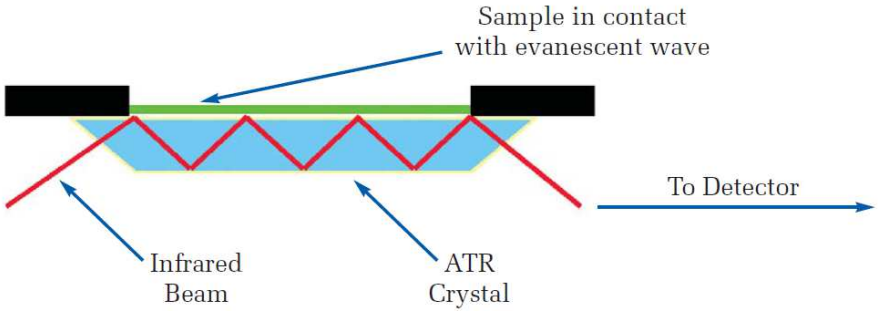


Figure 2.9: Schematic set-up for IR: infrared light is shone through an ATR crystal, where it interacts with a sample after which it goes to a detector [90].

One of the most used types of IR spectroscopy is attenuated total reflectance infrared spectroscopy (ATR-IR), this is an fast and easy way to measure an infrared spectrum of a material. The set-up is schematic shown in Figure 2.9; a sample is placed on a ATR crystal, which is a crystal with a high refractive index. A infrared beam is guided through the crystal to the interface at which the beam is totally reflected, however, the electric component of the light penetrates through the interface (which is called the evanescent wave). This energy be absorbed by the sample on the crystal; when this happens, the attenuated energy from the evanescent wave passes back to the infrared beam which then is measured by the detector. The signal obtained from during the measurement is subtracted from

the signal of the background measurement, where no sample was placed on the ATR crystal. This results in a IR spectrum[69,90]. From the spectral features that are shown in the IR spectrum information can be obtained about chemical bonds present in the material, since every chemical bond has its absorptions at specific wavelength regions.

**Measurements**
Infrared spectroscopy measurements were performed on a Tensor 37 spectrometer from Bruker with a MIRacle ATR stage from Pike. The spectra were measured between 4000-600 $cm^{-1}$ with a resolution of 4 $cm^{-1}$. Before each measurement a background scan was performed at ambient air, after which the powder was pressed on the ATR crystal. For each spectrum 32 scans were averaged.

### 2.4.3 $N_2$–Physisorption

This technique is used to determine the surface area and pore volume of a material; it is mostly used for porous materials, as they possess relative large surface areas and pore volumes. A material is dried under vacuum by heating to completely empty the pores before the measurement, then slowly a known amount of nitrogen is added to the system until all of the accessible pores are fully occupied by the nitrogen. By plotting the pressure divided by the condensation pressure (the pressure at which all pores were fully occupied) an isotherm is obtained from which the surface area and pore volume of the material can be calculated. From the isotherm it is also possible to see if there is any micro- or mesoporosity is present in the material[91].

**Measurements**
The physisorption measurements were performed using a Tristar 3000 V6.08 A from Micromeritics. First the samples were dried at 300℃ after which the isotherms were measured at -196℃. After the measurement the specific surface area and pore volumes were determined using the BET approach and by fitting the isotherm to a t-plot of alumina/silica.

### 2.4.4 Thermogravimetric Analysis

Thermogravimetric analysis (TGA) can be used to measure the thermal stability of a material. The mass of a material is measured while heating with a certain ramp over time. If there is anything loosely bound to the material, for example solvent molecules in a porous material, it will be released if the temperature is high enough which results in a decrease in mass. Also the thermal stability of the material can be measured by looking at the temperature at which the measured

mass has a huge decrease as result of the collapsing structure. The stabilities can be measured in different both ambient and inert atmospheres, which mostly leads to different thermal stabilities[92].

**Measurements**
For the TGA measurements a Q50 TGA from TA instruments was used. A platinum pan was first cleaned by heating with a blowtorch after which 10-15 mg sample was weighed. The TGA profiles were measured from room temperature to 1000℃ with a heating ramp of 5℃/min. under a 60 mL/min. $N_2$ stream.

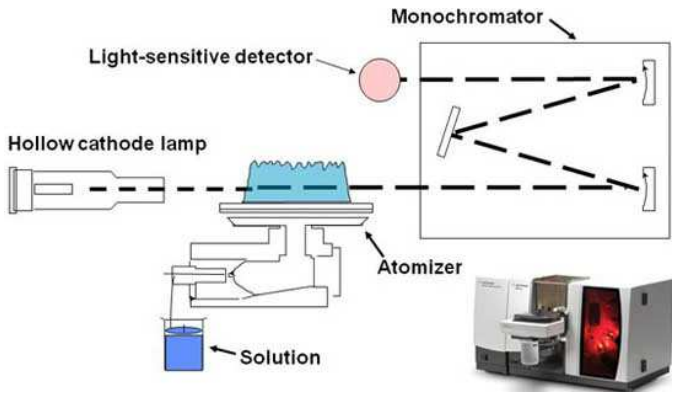


Figure 2.10: Schematic scheme of the AAS set-up, a lamp shines light through flame with the nebulised sample. The monochromator let pass only light of a certain energy which is measured by the detector[93].

### 2.4.5 Atomic Absorption Spectroscopy

Atomic Absorption Spectroscopy (AAS) is an analysis technique that can determine the elemental composition of a material both qualitatively and quantitatively using the absorption of light. In Figure 2.10 the schematic set-up for the AAS measurement is shown. An in water dissolved material is nebulised in a flame where the droplets evaporate after which the remaining solids in the solution first are vaporised, then atomised and finally ionised. Through the flame light is shined which can be absorbed by the ions, this is done by a hollow cathode lamp. Due to well defined energy levels for individual atoms, each element has its specific energies at which light is absorbed. The amount of light absorbed depends on the concentration of the element, which leads to the possibility to quantify the amount of an element present in the solution[69]. To determine the amount of an element present in the solution a calibration curve has to be made, a series of known concentrations has to be prepared and measured to obtain the calibration line from which the concentration of the samples can be obtained.

Table 2.1: Zinc and manganese concentrations used for calibration curve for the AAS measurements, to all solution demineralised water was added to a total volume of 10 mL.

| # | Zinc solution (mL) | concentration Zn ($mg \cdot L^{-1}$) | Manganese solution (µL) | concentration Mn ($\mu g \cdot L^{-1}$) |
|---|---|---|---|---|
| 0 (blank) | 0 | 0 | 0 | 0 |
| 1 | 0.1 | 0.10 | 40 | 41 |
| 2 | 0.3 | 0.29 | 60 | 61 |
| 3 | 0.5 | 0.49 | 80 | 82 |
| 4 | 0.7 | 0.69 | 100 | 102 |
| 5 | 1.0 | 0.98 | 300 | 307 |
| 6 | 1.2 | 1.2 | 500 | 511 |

**Measurements**
To measure the metal concentrations in the different samples a calibration curve had to be made. A stock solution for zinc was made by dissolving 61 mg ZnO in 2.5 mL concentrated nitric acid (65%) in a 50 mL volumetric flask which then was filled with demineralised water. For the manganese stock solution 66 mg MnO was dissolved in 10 mL concentrated nitric acid (65%) in a 50 mL volumetric flask filled with demineralised water. Both solutions were diluted 100 times separately by adding 1 mL of the solution in separate 100 mL volumetric flasks which than were filled with demineralised water, the final concentration of the stock solutions were the final concentration of the final stock solution was 9.8 $mg \cdot L^{-1}$ for zinc and 10.2 $mg \cdot L^{-1}$ for manganese. The calibration curves were made with the following concentrations (all solutions were made in 10 mL volumetric flasks). The blank solution was made by a diluting concentrated nitric acid with demineralised water.

The samples were prepared using the following method. First the samples were dried at 200℃ for 3 hours. Then 10 mg sample was weighed and dissolved in 2 mL concentrated nitric acid (65%) in a 10 mL volumetric flask after which the flask was filled with demineralised water. The solutions were diluted 400 times by adding 25 µL to a 10 mL volumetric flask and fill it to the line with demineralised water. For the transfer of all solutions Finn pipettes were used, except for determining the amount of concentrated nitric acid that was used. The pH of all solutions was adjusted to be between 1-3. For the measurements a ContrAA® 300 atomic absorption spectrometer from Analytik Jena was used. An acetylene/air flame was used which was optimised before every measurement, a xenon lamp was used as light source. For the zinc measurements the primary emission line at 213.86 nm was used, for manganese the primary emission line at 279.48 nm was used.

### 2.4.6 Electron Microscopy

To look at a material which is in the nanosize range, electron microscopy can be used. For obtaining information about the surface of a material Scanning Electron Microscopy (SEM) can be used; to look at the two dimensional nanostructures in more detail Transmission Electron Microscopy (TEM) can be used. Both techniques are schematically shown in Figure 2.11 [94]. SEM shoots a beam of electrons with an energy of ∼30 keV to the sample, those electrons can be reflected (which are called backscattered electrons) or can generate secondary electrons. The electron beam is focused into a point which scans the surface; creating both backscattered and secondary electrons which have their own detector collecting the electrons to generate an image. TEM uses an electron beam of 80-400 keV which goes through the sample, therefore a thin sample (∼20 nm) is required, and is collected by a detector at the other side. The electrons can be diffracted or scattered by the material which causes a contrast in the image; the thicker the sample or the heavier the atoms of the sample, the more electrons that are diffracted leading to a dark place on the image. It is also possible to measure TEM with a focussed beam and scan the material, this is called scanning transmission electron microscopy (STEM).

With electron microscopy it is possible to obtain information about the chemical composition of the material; Energy Dispersive X-ray spectrometry (EDX) can be used to identify different elements both qualitatively and quantitatively. An electron from the electron beam can knock out an electron from one of the inner shells of the atom creating a hole, one of the electrons in an outer shell can fall back to this vacancy. Due to the difference in energy between the two levels a photon is emitted which has an energy of X-rays. This energy is equal to the difference in energy between the two levels, this results in characteristic X-rays by which chemical mapping can be performed on the material.

**Measurements**

The SEM measurements were performed using a XL30 SFEG scanning electron microscope from Philips/FEI. The acceleration voltage for all measurements was 15 kV. The images were taken using the backscattered electrons. The SEM-EDX measurements were performed using an EDX detector from EDAX. The samples were prepared by placing a bit of the powder on a SEM sample holder covered with carbon tape.

For the TEM measurements (both bright field as HAADF imaging) a Tecnai 20FEG transmission electron microscope from Philips/FEI was used. The samples were prepared by first grinding the samples obtaining fine powders, then drying at 300℃ for 3h, finally a copper TEM grid was moved through the powder. The microscope was equipped with a EDX detector from EDAX for elemental analysis.

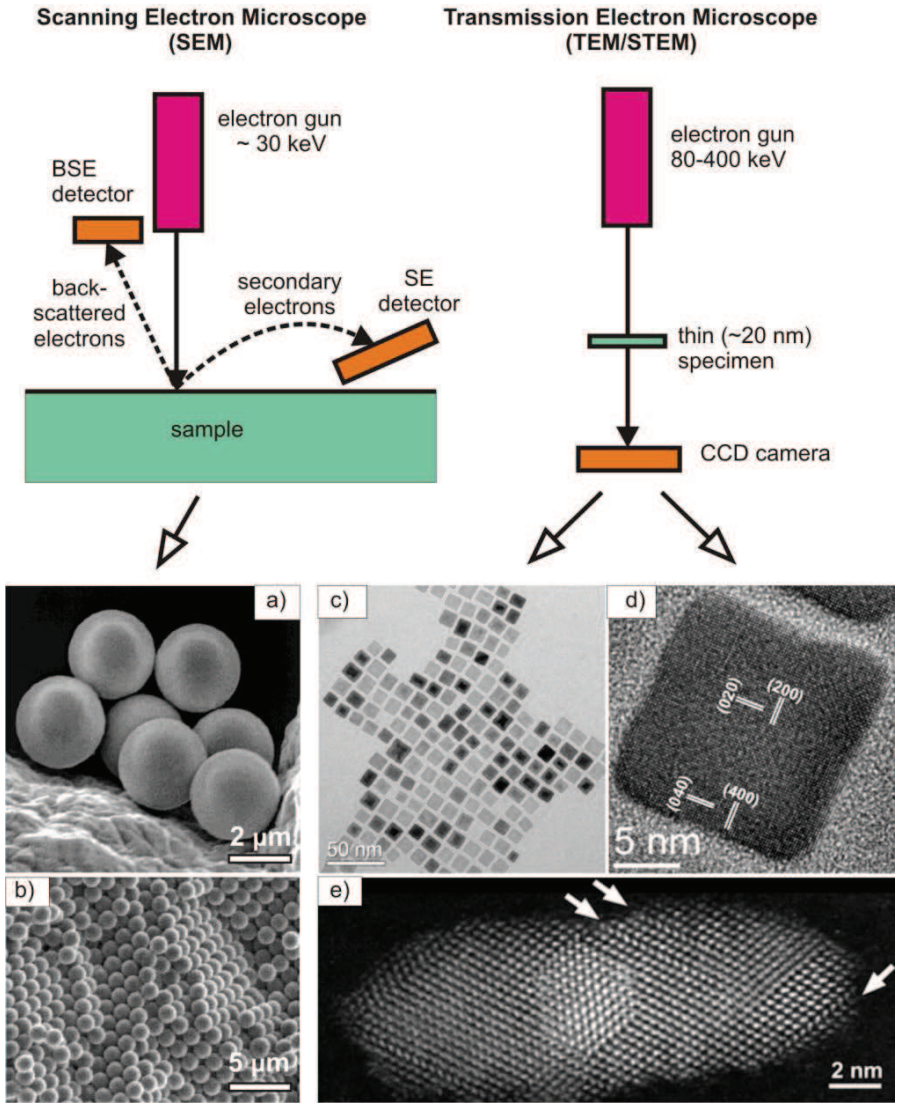


Figure 2.11: Schematic scheme of the principles of scanning and transmission electron microscopy; examples of images obtained with both SEM (a,b) and TEM (c,d,e) are shown [94].

# 3 Experimental methods

## 3.1 ZIF-8 synthesis

Before the metal-ion exchange could be performed the parent ZIF-8 material had to be synthesised. The three most used methods in literature for the synthesis of ZIF-8 were performed to see which resulted in the most promising candidate for the exchange reaction.

### 3.1.1 Chemicals used

- 2-methylimidazole [HMeIm, Acros Organics, 99$^+$%]
- Ammonia [$NH_4OH$, Merck, 25%]
- Chloroform [$CH_3Cl$, Interchema, Pract.]
- Dimethylformamide [DMF, Acros Organics, 99$^+$%]
- Methanol [MeOH, Interchema, Pract.]
- Zinc nitrate hexahydrate [$Zn(NO_3)_2{\cdot}6\,H_2O$, Sigma-Aldrich, ≥99%]
- Zinc nitrate tetrahydrate [$Zn(NO_3)_2{\cdot}4\,H_2O$, Merck, 98.5%]

### 3.1.2 ZIF-8 synthesis in DMF

$$Zn(NO_3)_2{\cdot}4\,H_2O \xrightarrow[\text{DMF, 24h, 140℃}]{\text{2-methylimidazole (HMeIm)}} \text{ZIF-8}\ \ (Zn(MeIm)_2)$$

Reaction equation for the synthesis of ZIF-8 in DMF.

$Zn(NO_3)_2{\cdot}4\,H_2O$ (0.210 g, 8.03x10$^{-4}$ mol) and HMeIm (0.060 g, 7.31x10$^{-4}$ mol) were dissolved in 18 mL DMF in a 20 mL vial which was capped. The capped vial was placed in an oven, the temperature was set to 140°C with a heating ramp of 5°C/min. It was kept at this temperature for 24h after which it was cooled at a rate of 0.4°C/min to room temperature. The mother liquor was removed by decanting and 2x 10 mL chloroform was added. After vigorously shaking and removing the crystals that were adsorbed on the glass of the vial, the suspension was filtrated. The crystals were washed with DMF (3x 10 mL) after which they were dried at room temperature[2]. The obtained crystals were submerged in methanol for 3 days refreshing the methanol every 24h after which they were dried at room temperature. Finally the solids were dried overnight in an oven of 70℃ with a heating ramp of 5℃/min.

### 3.1.3 ZIF-8 synthesis in methanol

$$Zn(NO_3)_2{\cdot}6\,H_2O \xrightarrow[MeOH,\ 24h,\ RT]{\text{2-methylimidazole (HMeIm)}} \text{ZIF-8}\ \ (Zn(MeIm)_2)$$

Reaction equation for the synthesis of ZIF-8 in methanol.

$Zn(NO_3)_2{\cdot}6\,H_2O$ (0.21 g, 7.06x$10^{-4}$ mol) was dissolved in 10 mL methanol, HMeIm (0.46 g, 8.04x$10^{-3}$ mol was dissolved in 10 mL methanol. The solutions were mixed in a 20 mL glass vial and shaken vigorously for 10 seconds, after which it was kept at room temperature for 24h. The crystals were obtained by centrifuging twice for 5 minutes at 4000 rpm and washed with 20 mL methanol. The crystals were dried at room temperature for one day and then dried overnight in an oven of 75℃ with a heating ramp of 5℃/min [24]. ZIF-8 was also synthesised on a 5 times larger scale using the same procedure by multiplying all amounts by 5.

### 3.1.4 ZIF-8 synthesis in concentrated aqueous ammonia

$$Zn(NO_3)_2{\cdot}6\,H_2O \xrightarrow[NH_4OH,\ 10min,\ RT]{\text{2-methylimidazole (HMeIm)}} \text{ZIF-8}\ \ (Zn(MeIm)_2)$$

Reaction equation for the synthesis of ZIF-8 in aqueous ammonia.

$Zn(NO_3)_2{\cdot}6\,H_2O$ (0.594 g, 2.01x$10^{-3}$ mol) was dissolved in 3.0 mL demineralised water, HMeIm (0.328 g, 4.00x$10^{-3}$ mol) was dissolved in 4.2 mL concentrated ammonia (25wt%). The two solutions were mixed in a 20 mL glass vial and stirred for 10 minutes at room temperature. The crystals were obtained by centrifuging at 4000 rpm for 5 minutes and washed with demineralised water until the pH of the supernatant reached a value of ∼7. The final product was dried in an oven at 60°C overnight after which it was dried at 200°C for 3h [62].

## 3.2 Post-synthetic cation exchange and direct synthesis of ZIF-8(Zn/Mn)

### 3.2.1 Chemicals used

- 2-methylimidazole [HMeIm, Acros Organics, 99$^+$%]
- Cobalt acetate tetrahydrate [$Co(OAc)_2{\cdot}4\,H_2O$, Acros Organics, 97%]
- Cobalt acetylacetonate [$Co(acac)_2$, Acros Organics, 99%]
- Cobalt chloride hexahydrate [$CoCl_2{\cdot}6\,H_2O$, Acros Organics, p.a.]

- Cobalt nitrate hexahydrate [$Co(NO_3)_2{\cdot}6\,H_2O$, Acros Organics, $99^+\%$]
- Copper acetylacetonate [$Cu(acac)_2$, Sigma-Aldrich, 97%]
- Copper chloride [$CuCl_2$, Merck, 98%]
- Copper nitrate trihydrate [$Cu(NO_3)_2{\cdot}3\,H_2O$, Sigma-Aldrich, 99%]
- Dimethylformamide [DMF, Acros Organics, $99^+\%$]
- Manganese acetate tetrahydrate [$Mn(OAc)_2{\cdot}4\,H_2O$, Acros Organics, $99^+\%$]
- Manganese acetylacetonate [$Mn(acac)_2$, Sigma-Aldrich, purity not specified]
- Manganese chloride tetrahydrate [$MnCl_2{\cdot}4\,H_2O$, Sigma-Aldrich, $98^+\%$]
- Manganese nitrate tetrahydrate [$Mn(NO_3)_2{\cdot}4\,H_2O$, Sigma-Aldrich, $97^+\%$]
- Manganese oxide [MnO, Sigma-Aldrich, $99^+\%$]
- Methanol [MeOH, Interchema, Pract.]
- Methanol anhydrous [MeOH, Sigma-Aldrich, 99.8%]
- Nitric acid [$HNO_3$, Merck, 65%]
- Zinc nitrate hexahydrate [$Zn(NO_3)_2{\cdot}6\,H_2O$, Sigma-Aldrich, $\geq$99%]
- Zinc oxide [ZnO, Sigma-Aldrich, $99^+\%$]

### 3.2.2 Direct synthesis of ZIF-8(Zn/Mn)

$$Zn(NO_3)_2{\cdot}4\,H_2O + Mn^{2+}\text{precursor} \xrightarrow[\text{DMF, 24h, 140℃}]{\text{2-methylimidazole (HMeIm)}} \text{ZIF-8(Zn/Mn)}$$

Reaction equation for the direct synthesis of ZIF-8(Zn/Mn)

$Zn(NO_3)_2{\cdot}6\,H_2O$ (215 mg, 0.73 mmol), HMeIm (60 mg, 0.73 mmol) and $Mn^{2+}$ (0.07 mmol, 17.2 mg for $Mn(OAc)_2{\cdot}4\,H_2O$; 17.7 mg for $Mn(acac)_2$; 13.9 mg for $MnCl_2{\cdot}4\,H_2O$; 17.6 mg for $Mn(NO_3)_2{\cdot}4\,H_2O$) were dissolved in 18 mL DMF in a 20 mL glass vial. The vial was capped and placed in an oven which was set with a heating ramp of 5℃/min at 140°C at which they were kept for 24h. After cooling the mother liquor was removed by decanting and the crystals were filtered and washed with chloroform (3x 10 mL). The obtained particles were submerged in 15 mL chloroform for 3 days, refreshing the chloroform every 24h. The chloroform was removed and the solids were dried at room temperature for 3 days and then dried under vacuum overnight [23].

### 3.2.3 Cation exchange in ZIF-8

In the general procedure, $Mn(acac)_2$ (150 mg, 0.6 mmol) was dissolved in methanol (5 mL), to get it well dissolved an ultrasonic bath was used, obtaining a concentration of 0.12 M. This solution was added to ZIF-8 (45 mg, 0.22 mmol equivalent of Zn) and placed in a preheated oven of 55℃ for 24h. After cooling the crystals were obtained by centrifuging at 3500 rpm for 7 minutes, the solution was decanted and the crystals were washed with fresh methanol until the supernatant was colourless.

The solids were submerged in methanol for 3 days, refreshing the methanol every 24h. After 3 days the methanol was removed and the solids were dried overnight at room temperature and then overnight at 75℃[23].

The cation exchange is also performed under inert conditions. In a typical procedure, $Mn(acac)_2$ (300 mg, 1.2 mmol) was placed in a schlenk flask. The flask was placed under inert conditions by evacuating the flask and purging with argon 5 times. In a glove box 10 mL of anhydrous methanol was added to the flask in which the $Mn(acac)_2$ was dissolved with help of an ultrasonic bath. ZIF-8 (90 mg, 0.44 mmol equivalent of Zn) was placed in a flask under inert conditions also by evacuating and purging with argon 5 times. The dissolved manganese solution was transferred to the flask with ZIF-8 by use of a cannula. The mixture was heated by a preheated oil bad at 55℃ for 24h while stirring at 350 rpm. The crystals were collected by centrifuging at 4000 rpm for 10 minutes and washed with 15 mL methanol twice. The solids were submerged in methanol for 3 days, refreshing the methanol every 24h. After 3 days the methanol was removed and the crystals were dried overnight at room temperature and then overnight at 70℃.

Different parameters were investigated during the research, in Table 3.1 all parameters are shown.

Table 3.1: Different parameters used for the metal-ion exchange.

| | |
|---|---|
| Metal-ions | Cobalt(II), Copper(II) & Manganese(II) |
| Time | 1 day, 3 days, 6 days & 2 weeks |
| Temperature | RT, 55℃ & 80℃ |
| Solvents | DMF, Methanol & Water |
| $Zn^{2+}$ : $Mn^{2+}$ ratio | 1:1, 1:3 & 1:6 |
| Atmosphere | Inert & Ambient |
| pH | <7, 7 & 7< |

# 4 Results and Discussion

## 4.1 ZIF-8 synthesis

ZIF-8 has been synthesised in different solvents, it has been performed in dimethylformamide, methanol and aqueous ammonia. To see which synthesis method resulted in the most promising candidate for the metal-ion exchange reaction, several analysis techniques were used to characterise the different ZIF-8 products.

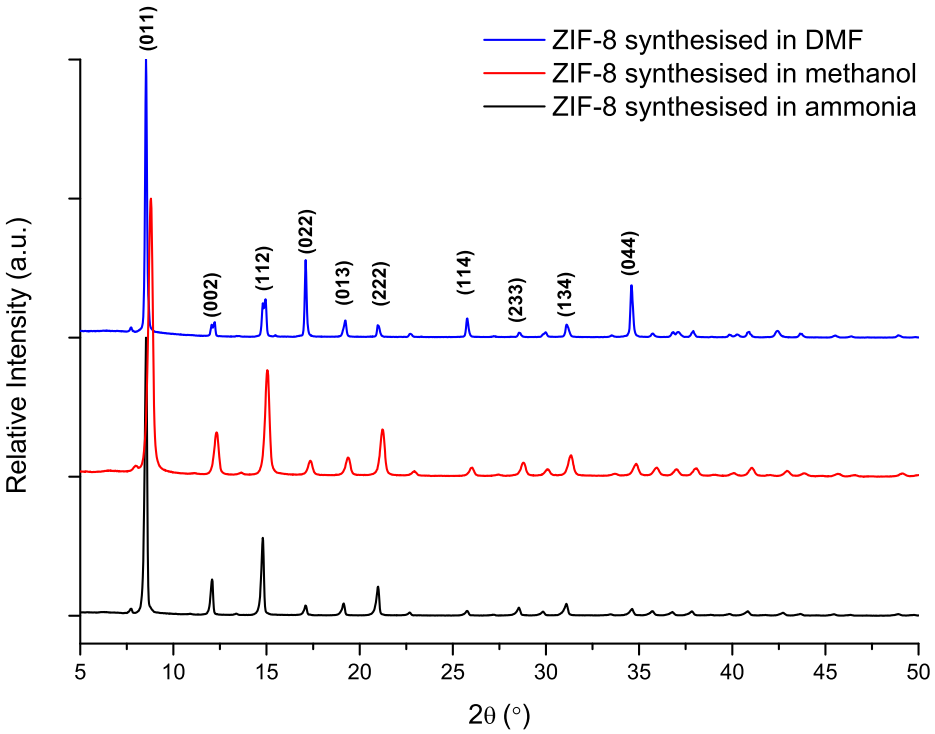


Figure 4.1: X-ray diffractograms of ZIF-8 synthesised in different solvents (Blue is synthesised in DMF; red in methanol; black in aqueous ammonia). The different diffractograms show the same peak patterns from which can be concluded that the different powders have a similar crystallinity and crystal structure.

The crystallinity and crystal structure of the different synthesised solids were determined using X-ray diffraction (XRD). In Figure 4.1 the diffractograms of the solids synthesised in different solvents are shown. All three methods resulted in highly crystalline products. The same peaks are observed in the three diffractograms from which can be concluded that the different synthesis methods results in isostructural products. XRD diffraction patterns in literature confirm that the synthesised products have the ZIF-8 crystal structure[2,24,50]. A difference in the

ratio of the peak intensities for ZIF-8 synthesised in DMF is observed when compared to the peak ratios in the diffractograms of the synthesis in methanol and aqueous ammonia. For example the (022) and (044) plane have a relatively higher intensity for the synthesis in DMF[2,24]. This indicates that the preferred directional growth for ZIF-8 in DMF is different from the preferred directional growth in other solvents, which is due to the coordination of DMF to the ZIF-8 framework during the synthesis.

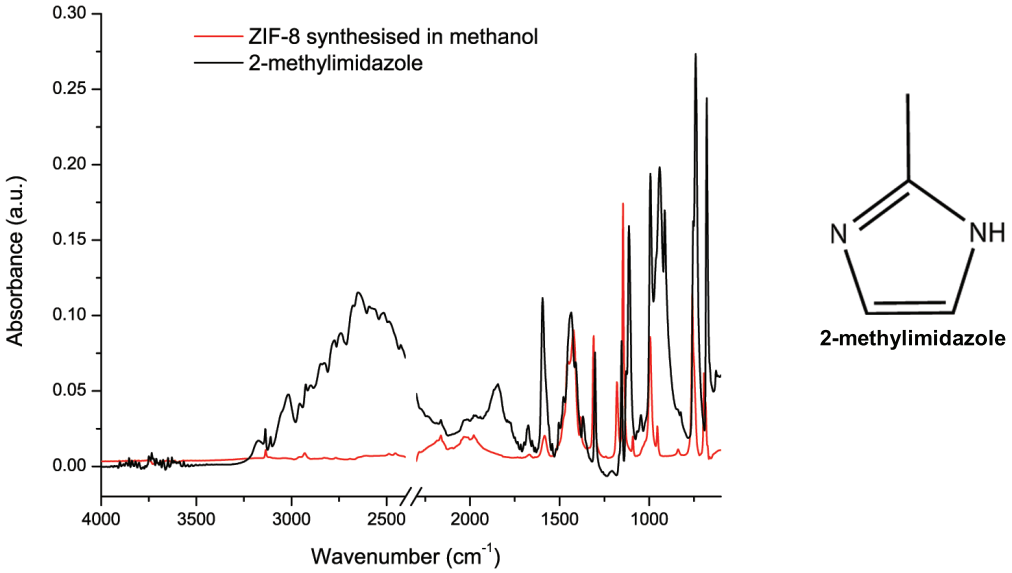


Figure 4.2: Infrared spectra of 2-methylimidazole (black) and the synthesised ZIF-8 (red). The band assigned to the H−N···H hydrogen bridge has disappeared in the ZIF-8 spectrum, indicating that the nitrogen atoms in HMeIm are coordinated to the zinc(II) ions.

To confirm that there wasn't any unreacted 2-methylimidazole left in the obtained ZIF-8 Fourier transform infrared spectroscopy (FTIR) was used. In Figure 4.2 the infrared spectra of 2-methylimidazole (black) and ZIF-8 synthesised in methanol (red) are shown. In the spectrum of 2-methylimidazole a broad band from 3250 $cm^{-1}$ to 2200 $cm^{-1}$ is present, which can be assigned to the H−N···H hydrogen bridge[95]. Also the band at 1850 $cm^{-1}$, which is the resonance between the H−N···H out-of-plane bending vibration and the N−H stretch vibration, can be assigned to 2-methylimidazole. From the absence of those two bands can be concluded that there isn't any unreacted HMeIm left in the product. The 2-methylimidazole was deprotonated during the synthesis and is coordinated to the zinc(II) ions and the unreacted HMeIm has been removed from the product with the washing steps.

To compare the three different ZIF-8 products, the IR spectra of the synthesised

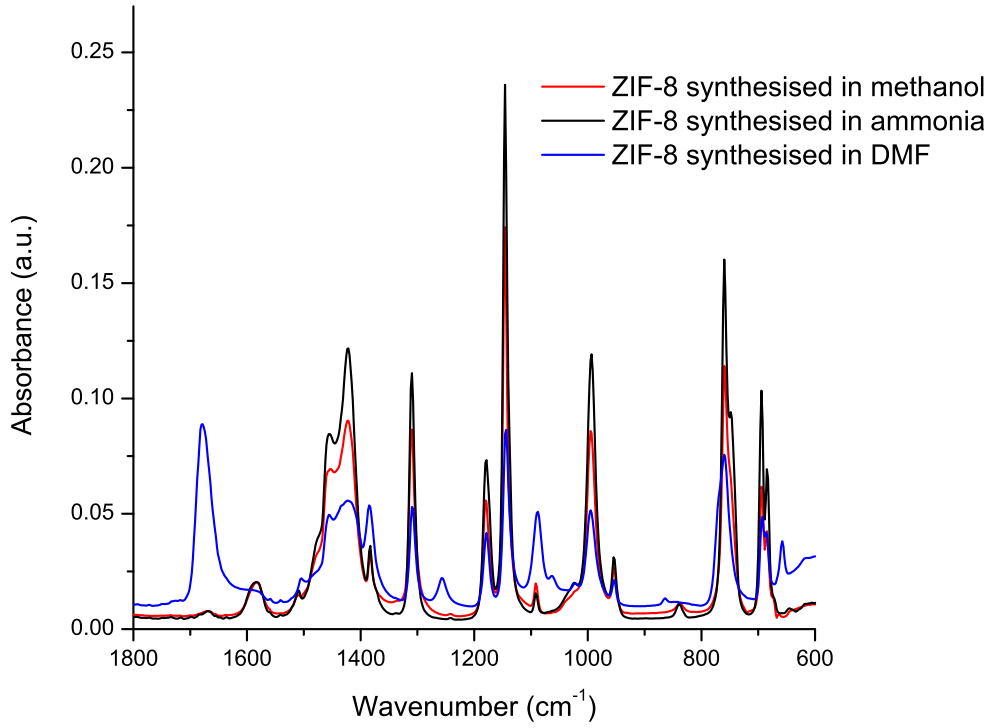


Figure 4.3: Infrared spectra of ZIF-8 synthesised in DMF (blue) aqueous ammonia (black) and methanol (red). The same spectral features are present in the three different spectra, indicating that the same chemical bonds are present in the different solids. In the spectrum of ZIF-8 synthesised in DMF three bands (1675 $cm^{-1}$, 1256 $cm^{-1}$ and 660 $cm^{-1}$) are visible which means that there is still some DMF left in the pores.

ZIF-8 are shown in Figure 4.3. The same spectral features are presented in the different spectra indicating that the same characteristic vibrations are present in the three products. All spectral features are in agreement with the literature[96,97]. In the spectrum of ZIF-8 synthesised in DMF four bands of DMF are shown (at 1675 $cm^{-1}$ (C=O stretch), 1256 $cm^{-1}$ (N−$CH_3$ stretch), 1063 $cm^{-1}$ (C−H bend) and 660 $cm^{-1}$ (N−C=O)), this indicates that the DMF is not completely removed from the product upon exchanging with methanol and drying of the solid. A complete assignment of the spectral features observed in all infrared spectra can be found in Table A.1.

The thermal stability of the three synthesised ZIFs was determined using thermogravimetric analysis (TGA). In Figure 4.4 the TGA profiles of the three synthesised ZIFs are presented. In the curve of ZIF-8 synthesised in DMF (blue) a decrease in mass is observed around 150-210℃. This decrease (20%) is due to the

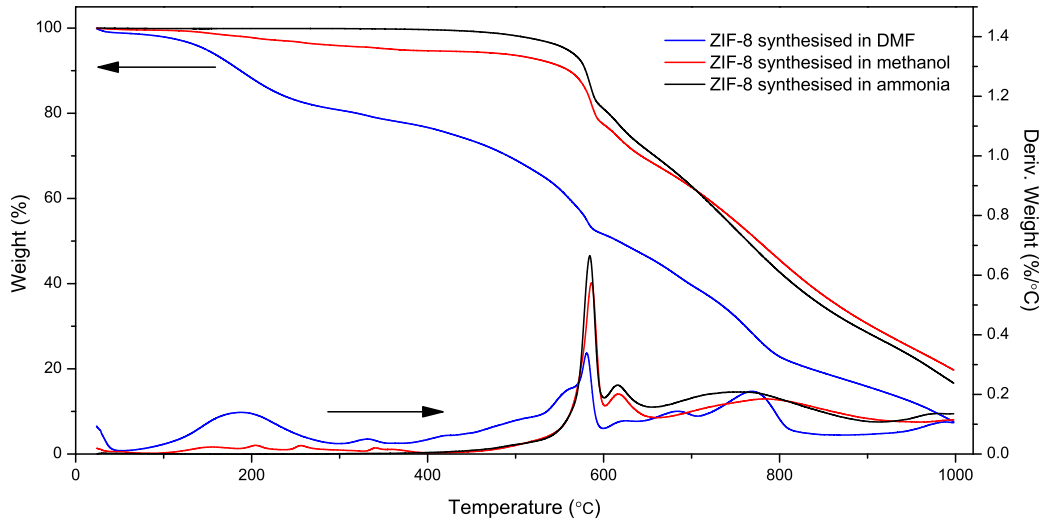


Figure 4.4: TGA curves of ZIF-8 synthesised in DMF (blue), methanol (red) and aqueous ammonia (black). The curve with DMF shows a drop around 180℃ indicating that DMF was still in the pores. The thermal stability of the different synthesised ZIF-8 is up to 587℃.

DMF, that was present in the pores coordinating to the framework, evaporating and leaving the pores of the material. All structures have a huge decrease in mass starting at 587℃, which is due to the organic linker that is burned leading to the collapse of the crystal structure. Based on this, it can be concluded that the thermal stability of the synthesised ZIFs are comparable with 587℃.

Scanning electron microscopy (SEM) was used to get visual understanding of the synthesised particles. In Figure 4.5 the SEM images of the different ZIF-8 products are shown. The ZIF-8 particles obtained by the synthesis in DMF (Figure 4.5a & b are big particles with a size of ± 100-200 µm. On the surface of the crystal smaller particles with a size around 10 µm are present. This probably is the result of the unfinished reaction after the synthesis, a longer reaction time might be needed to obtain flat surfaces. The synthesis in aqueous ammonia (Figure 4.5c & d resulted in cubic particles with an average size of 700 nm. The particles have a flat surface, the ammonia which was added to the reaction mixture deprotonated the 2-methylimidazole linker resulting in a shorter time needed to complete the reaction [47], compared to the reaction in DMF. The smallest particles were obtained with the synthesis in methanol (Figure 4.5e & f). On first sight it looked like a big particles has formed with some small particles present, but when looked in more detail in small hexagonal shaped particles with an average size of 80 nm are observed.

Now a full characterisation of ZIF-8 synthesised in DMF, aqueous ammonia

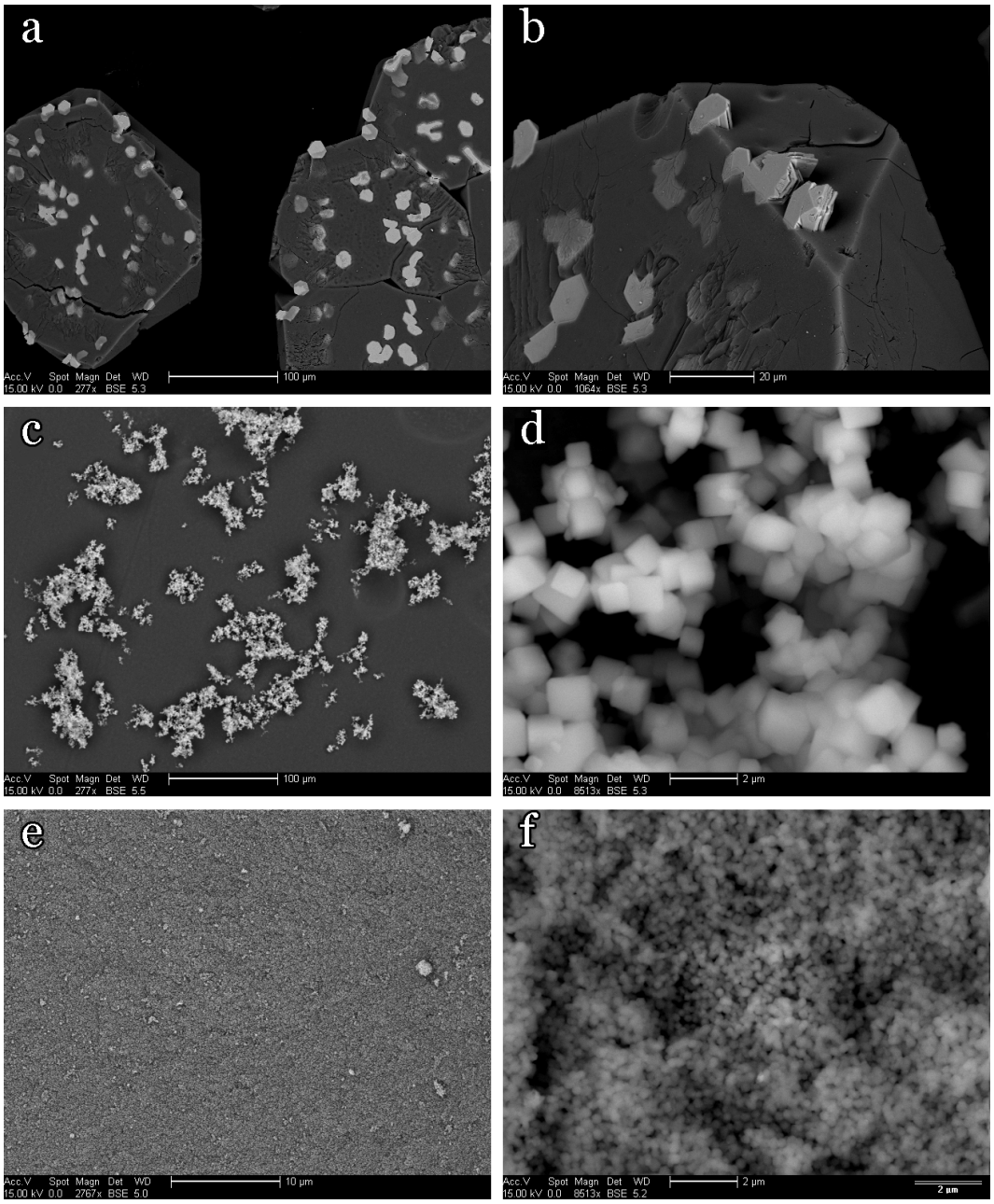


Figure 4.5: SEM pictures of ZIF-8 synthesised in DMF (a & b); in aqueous ammonia (c & d); in methanol (e & f). Big particles with a size of ± 100-200 µm with smaller particles on the surface were obtained for the synthesis in DMF. Cubic particles with a size of ± 700 nm were obtained with the synthesis in aqueous ammonia. Hexagonal shaped particles with a size of ± 80 nm were synthesised in methanol.

and methanol has been done, the most promising candidates for the metal-ion exchange can be chosen. All synthesis methods resulted in white particles which possess the ZIF-8 crystal structure, as confirmed by XRD. The infrared spectra also confirm that ZIF-8 has been synthesised, the only difference is the presence of DMF in the pores of ZIF-8 synthesised in DMF. With 587℃ the thermal stability of all products is comparable to the thermal stability reported in literature, which is higher than most MOFs. For visual understanding of the particles SEM was used, in the images of ZIF-8 synthesised in DMF big particles ($\sim$150 µm) were seen with small particles present on the surface. The images of ZIF-8 synthesised in aqueous ammonia and methanol showed smaller particles ($\sim$ 700 nm and $\sim$ 80 nm respectively) with smooth surfaces. Taking into account the size and morphology of the particles, the most promising candidates for the metal-ion exchange were obtained by the synthesis in aqueous ammonia and methanol, which resulted in small particles with flat surfaces. Those two products were used for PSM during this research.

## 4.2 Direct synthesis of ZIF-8(Zn/Mn)

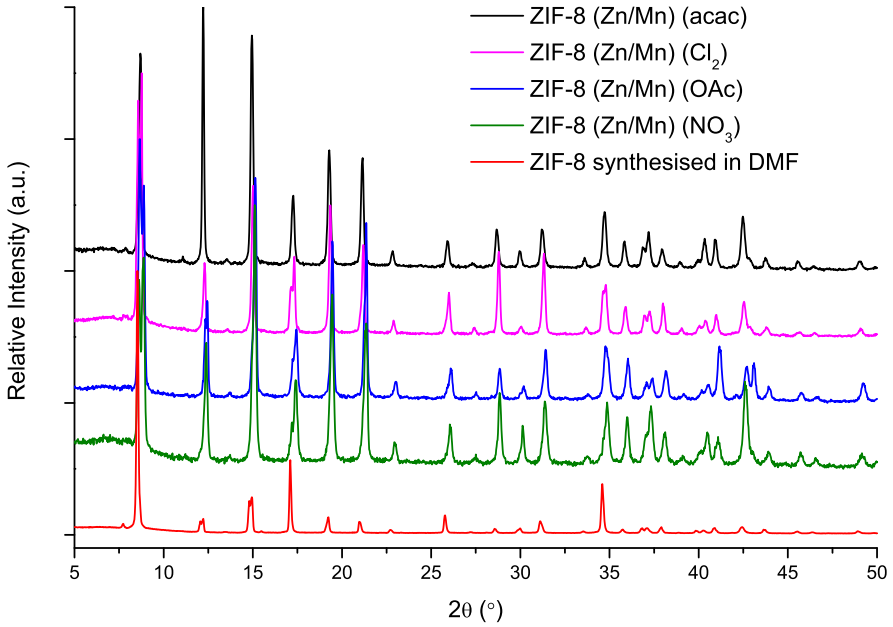


Figure 4.6: X-ray diffractograms of ZIF-8(Zn/Mn) obtained from the direct synthesis of ZIF-8 with different manganese precursors present during the synthesis: $Mn(acac)_2$ (blue), $MnCl_2$ (orange), $Mn(OAc)_2$ (pink), $Mn(NO_3)_2$ (black). The diffractogram of pure ZIF-8 synthesised in DMF (red) is added for comparison. The same peaks are observed in the diffractograms, it can be concluded that the different products possess the ZIF-8 crystal structure.

To see if ZIF-8 with manganese(II) incorporated in the framework can be synthesised directly or not, the synthesis of ZIF-8 was performed in the presence of different manganese(II) precursors. After the synthesis a light brown powder was obtained. To confirm that the products of this method have the ZIF-8 crystal structure X-ray diffraction was performed. In Figure 4.6 the diffractograms of the products obtained with the synthesis using different manganese precursors are shown, the diffractogram of pure ZIF-8 synthesised in DMF (red) is added for comparison. The intensities were normalised for better visualisation of the peak patterns, in Figure A.3 the original diffractograms are shown. The same peak patterns are observed in the diffractograms of the different products and the parent ZIF-8. Based on this observation, it can be concluded that the direct synthesis of ZIF-8(Zn/Mn) resulted in the ZIF-8 crystal structure. However, as can be seen in Figure A.3, the peak intensities are lower for ZIF-8(Zn/Mn) indicating that the crystallinity is lower compared to the crystallinity of the pure ZIF-8. This

might be due to the preferred octahedral coordination of $Mn_2^+$ which is forced in a tetrahedral coordination.

The chemical vibrations present in ZIF-8(Zn/Mn) were characterised using FTIR, in Figure 4.7 the spectra of the direct synthesised products are shown, the spectrum of ZIF-8 synthesised in DMF is added for comparison. The same characteristic bands are observed in the different spectra, from which can be concluded that the same chemical bonds (and no extra bonds) are present in the different products. The bands belonging to DMF are also present in the ZIF-8(Zn/Mn) products, meaning that DMF wasn't completely expelled from the pores of the products by the drying with vacuum.

Now we can conclude from XRD and FTIR that the direct synthesis method resulted in particles with the ZIF-8 crystal structure with the same characteristic vibrations. To determine the manganese to zinc molar ratio in the particles atomic absorption spectroscopy (AAS) was used. Unfortunately only zinc was observed in the synthesised ZIF-8(Zn/Mn) particles and no manganese content was found in the particles. From this result can be concluded that it isn't possible to synthesise ZIF-8(Zn/Mn) directly with DMF assisted solvothermal synthesis and post-synthetic modification by metal-ion exchange has to be performed to obtain ZIF-8 with manganese incorporated in the framework.

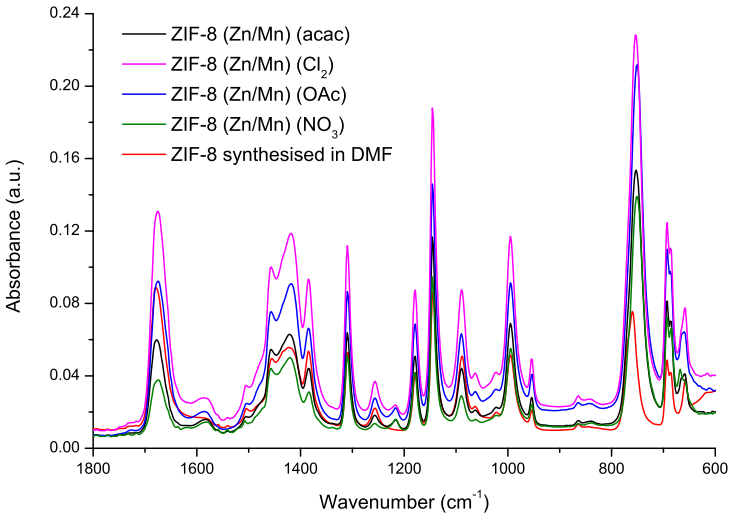


Figure 4.7: IR spectra of ZIF-8(Zn/Mn) obtained from the direct synthesis of ZIF-8 with different manganese precursors present during the reaction: $Mn(acac)_2$ (blue), $MnCl_2$ (orange), $Mn(OAc)_2$ (pink), $Mn(NO_3)_2$ (black). The spectrum of pure ZIF-8 synthesised in DMF (red) is added for comparison. The same spectral features are observed in all spectra, indicating that the same chemical bonds are present in the different products.

## 4.3 Metal-ion exchange in ZIF-8

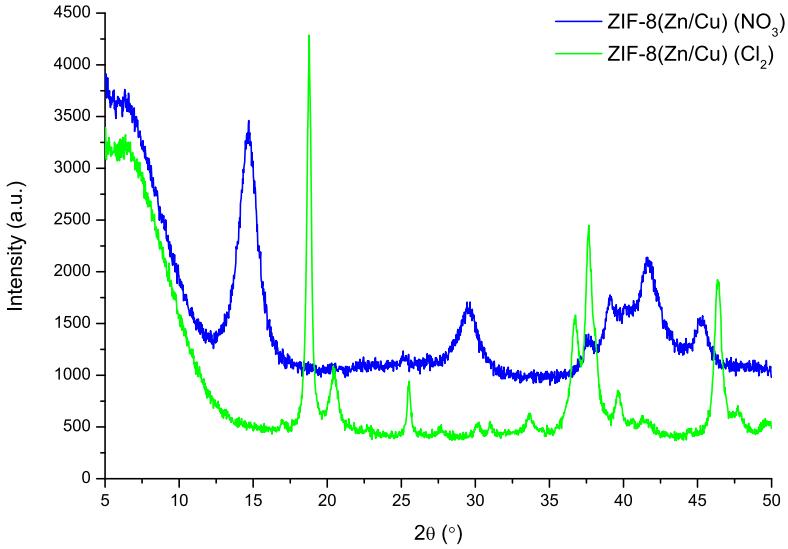


Figure 4.8: X-ray diffractograms of ZIF-8 exchanged with $Cu(NO_3)_2{\cdot}3\,H_2O$ (blue) and $CuCl_2$ (green). The crystal structure of ZIF-8 changed upon exchanging the zinc(II) ions by copper(II) ions.

Since it is not possible to directly synthesise ZIF-8 with manganese incorporated in the framework, post-synthetic modification (in this case metal-ion exchange) can be a powerful method to synthesise the desired materials. In this research metal-ion exchange is performed using three different metal-ions: copper, cobalt and manganese.

The effect of the pH on the metal-ion exchange was studied by addition of an acid (hydrochloric acid) or a base (sodium hydroxide) to the reaction mixture to find the optimal pH for the metal-ion exchange reaction. With the addition of a base to the reaction mixture, precipitation of metal oxides and metal hydroxides was immediately observed. Addition of an acid to the reaction mixture led to the protonation of ZIF-8 resulting in the dissolution of ZIF-8. Where the pH of the mixture was acidic before the addition of ZIF-8, it increased to 7 when ZIF-8 was added. From this results can be concluded that a pH $\sim$7 is the most promising for metal-ion exchange with ZIF-8.

Cation-exchange with cobalt(II), copper(II) and manganese(II) precursors on ZIF-8 has been performed. In Figure 4.8 the diffractograms of ZIF-8 exchanged with copper(II) nitrate and copper(II) chloride are shown. The peak patterns are different compared to the peak pattern of the parent ZIF-8 (shown in Figure 4.1). From this can be concluded that the crystal structure has changed during the

exchange reaction with copper(II). This might come due to the preferred octahedral geometry of $Cu^{2+}$ which disturbs the ZIF-8 crystal structure when exchanging the tetrahedrally coordinated zinc(II)-ions by the copper(II)-ions [98,99].

In the diffractograms of ZIF-8 exchanged with manganese(II) and cobalt(II) (Figure 4.9) the same peak patterns were obtained for the exchanged samples as for the parent ZIF-8 synthesised in methanol. From this can be concluded that the crystal structure of ZIF-8 has been retained after the exchange with cobalt and manganese with a comparable crystallinity of the materials. In the infrared spectra (showed in Figure 4.10) the same spectral features are shown for the different materials, indicating that the same chemical bonds are present in the samples.

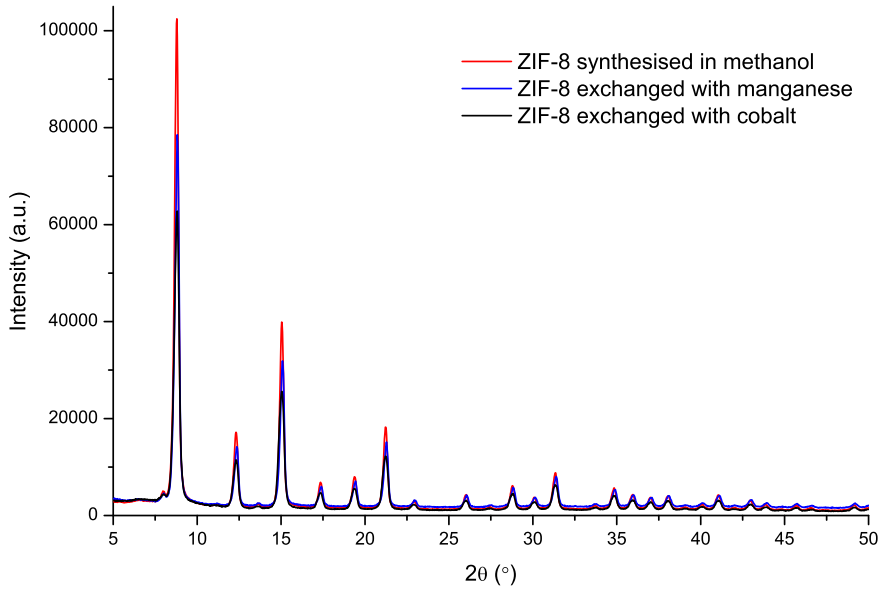


Figure 4.9: X-ray diffractograms of the parent ZIF-8 synthesised in methanol (red), ZIF-8 exchanged with manganese (blue) and ZIF-8 exchanged with cobalt (black). The same peak patterns are observed in the different diffractograms, from which can be concluded that the crystal structure of ZIF-8 has retained upon the metal-ion exchange with manganese(II) and cobalt(II).

To check if the unreacted cobalt(II)/manganese(II) acetylacetonate was removed from the product upon washing, the infrared spectra of both ZIF-8 exchanged with manganese and the pure manganese acetylacetonate were measured and compared. The spectra, including the spectrum of the parent ZIF-8, are shown in Figure 4.11. Three characteristic bands for manganese acetylacetonate are highlighted; 1604 $cm^{-1}$, 1018 $cm^{-1}$ and 919 $cm^{-1}$. From the absence of those bands (especially the band at 1604 $cm^{-1}$ which represents the C−O stretch vibration) in the spectra of ZIF-8 after the exchange reaction can be concluded that

there isn't any unreacted manganese acetylacetonate left in the product. Also no additional bands, compared to the parent ZIF-8, are observed indicating that no additional bonds are present after the reaction.

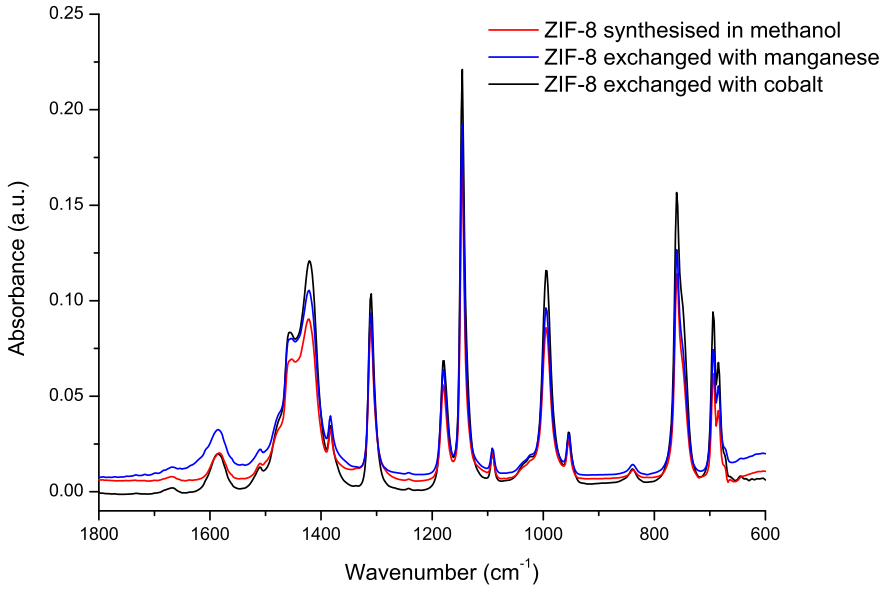


Figure 4.10: Infrared spectra of ZIF-8 exchanged with manganese (blue) and cobalt (black). For comparison the IR spectrum of the parent ZIF-8 synthesised in methanol has been added (red). The same spectral features are observed in the different spectra without extra bands indicating that the same chemical bonds are present in the materials and no additional bonds are present.

Incorporation of other metal-ions in the ZIF-8 framework might decrease the thermal stability of the material, as an other cation is introduced which is more reactive than the zinc(II)-ions in the framework. To see if the thermal stability has decreased after the exchange reaction thermogravimetric analysis was performed on ZIF-8 exchanged with manganese. In Figure 4.12 the TGA profiles of ZIF-8 (red), ZIF-8 exchanged with manganese (blue) and $Mn(acac)_2$ (pink) are shown. There is a slight decrease in thermal stability for ZIF-8 after the exchange reaction (577℃ for ZIF-8 exchanged with manganese compared to 587℃ for pure ZIF-8) but it still has a high thermal stability when compared to most other MOFs [100,101]. This decrease in thermal stability might be due to the disturbance of the framework by the incorporation of manganese in the ZIF-8 framework.

Although the exchanged product is thermally stable up to 577℃, the crystal structure of the solids might change with increasing temperature. To see whether this is the case high temperature XRD patterns were measured for ZIF-8 after the exchange reaction with manganese. The powder was placed in a cell which could

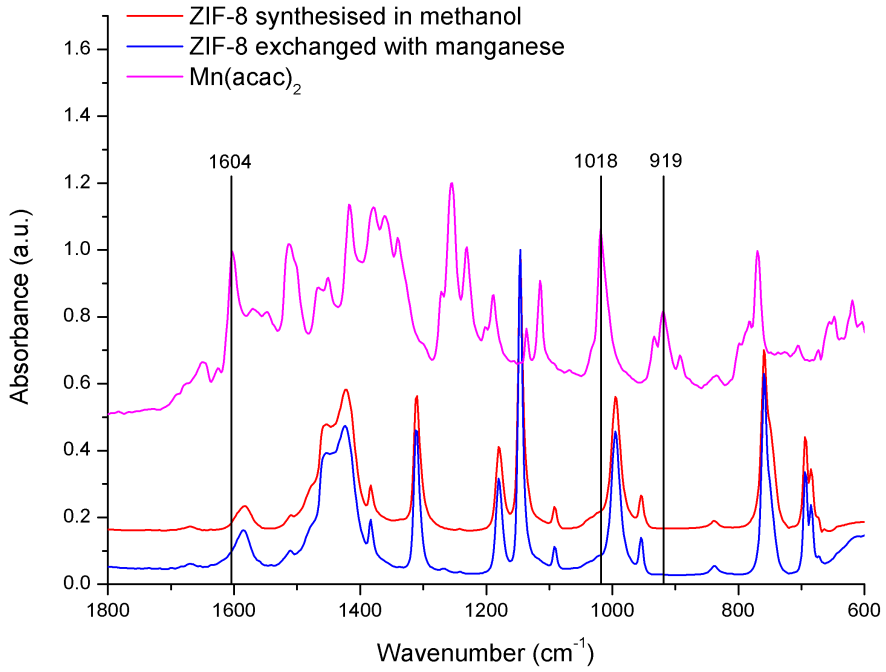


Figure 4.11: Infrared spectrum of ZIF-8 (red), ZIF-8 exchanged with manganese (blue) and $Mn(acac)_2$ (pink). Three characteristic bands for $Mn(acac)_2$ are highlighted, those bands aren't present in the spectrum for the manganese exchanged ZIF-8. The unreacted $Mn(acac)_2$ has been removed after the reaction by the washing steps.

be heated under inert atmosphere (helium was used for this experiment). The sample was heated to 100℃, starting at this temperature diffraction pattern were measured at constant temperature every 50℃ until 500℃, after which the sample was cooled to 30℃ at which the diffraction pattern was also measured. In Figure 4.13 the XRD pattern measured at 100℃, 500℃ and at 30℃ (after cooling) are shown. The same peak patterns and peak ratios are observed for the diffractograms measured at the different temperatures. So it can be concluded that the crystal structure of ZIF-8 doesn't change while heating up to 500℃. The diffractograms measured at all temperatures during the experiment can be found in Figure A.4.

With the full characterisation of the ZIF-8 particles after the exchange with different metal-ions it can be concluded that the exchange reaction of ZIF-8 with copper(II) leads to a change in the crystal structure. After the exchange reaction with cobalt and manganese the crystal structure of ZIF-8 is retained (XRD), the same (and no additional) chemical bonds are present in the solids (FTIR) and the thermal stability is comparable to the parent ZIF-8 particles (TGA). Now the metal rates have to be determined, this is analysed using atomic absorption

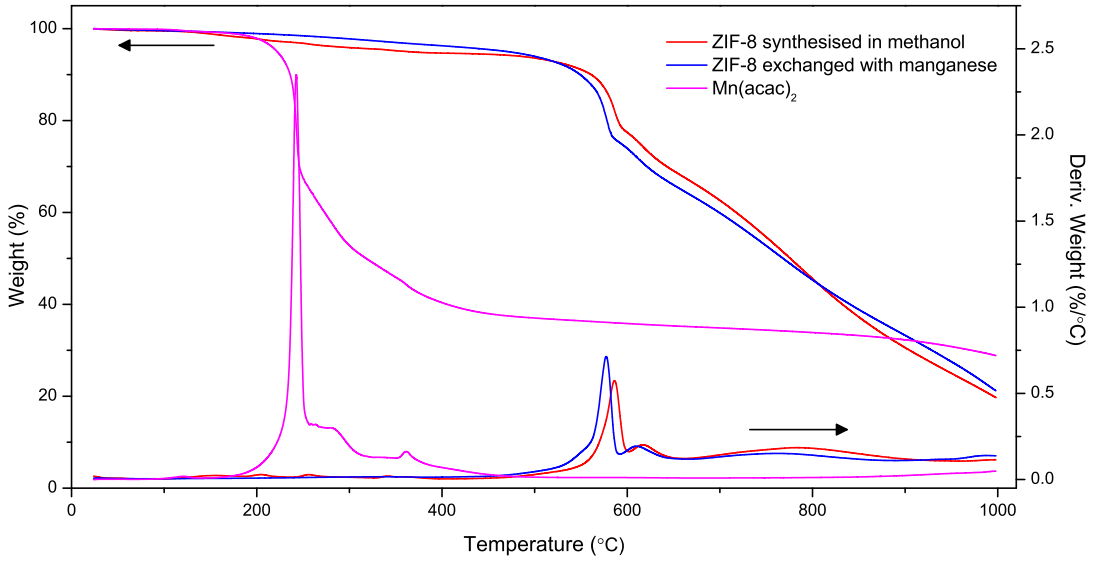


Figure 4.12: Thermogravimetric analysis of ZIF-8 exchanged with manganese (blue) compared with pure ZIF-8 (red). The thermal stability of ZIF-8 did not decrease significant upon metal-ion exchange with manganese. To show that no $Mn(acac)_2$ is adsorbed on the surface the TGA profile for $Mn(acac)_2$ (pink) is shown which is thermally stable up to 240°C.

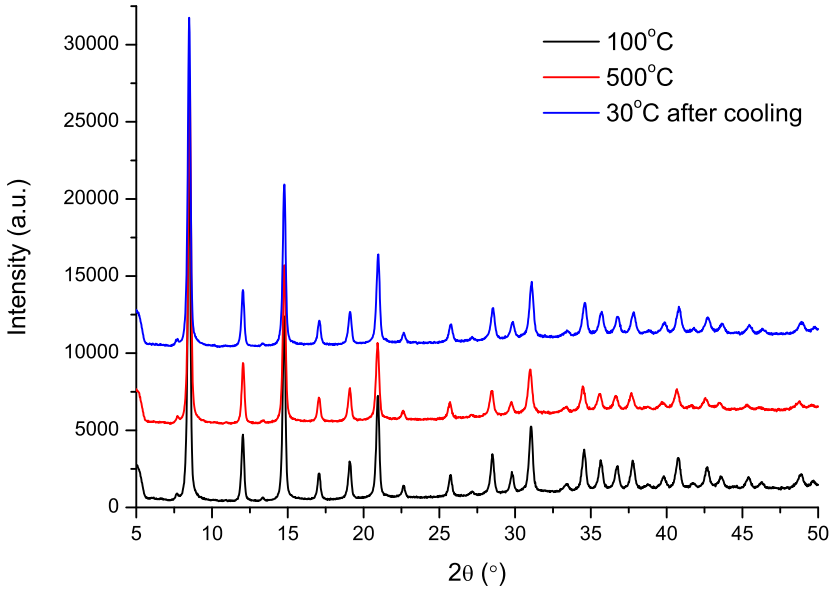


Figure 4.13: X-ray diffraction of ZIF-8 exchanged with manganese measured while heating up to 500°C. No change in crystallinity or crystal structure is observed during the experiment.

spectroscopy (AAS).

For the samples on which exchange reactions with cobalt was performed negligible cobalt concentrations were observed. Also the exchange reaction performed under inert conditions resulted in negligible manganese rates. For the exchange reactions performed with methanol and DMF as solvent under ambient conditions, similar exchange rates were observed. However, for the exchange reactions performed in water AAS analysis could not be performed, the samples didn't dissolve in nitric acid during the preparation. Which made it impossible to measure the metal concentrations with AAS. When only incorporation of manganese has taken place during the reaction the material should easily dissolve in nitric acid as the nitrogen atoms of the imidazole linker gets protonated in acidic medium. This indicates that other manganese species (for example oxides or hydroxides) have adsorbed on the surface of the framework instead of the incorporation of manganese(II) into the framework. The exchange reaction in DMF and methanol at room temperature led to similar results for the exchange rates, which makes methanol more favourable to use looking at the environmental aspects.

The average manganese rates obtained after the exchange reactions are shown in Figure 4.14. The rates are sorted on the different reaction times and temperatures used. The minimum and maximum values for the manganese rates for every reaction condition are shown with the bars. This shows that a wide variety of manganese rates is obtained when using the same reaction conditions. For example, the exchange reaction for 3 days at 55℃ resulted in an average manganese rate (based on the total metal content) of 13.1 mol%, based on 26 samples. The values of the exchange rates for this method differ between 2.0 and 32.3 mol%, which are deviations of 11.1 and 19.2 mol% respectively. Despite the big deviations for the exchange rates, a trend can be seen for the exchange rate based on time and temperature. An increasing manganese rate is observed when the reaction was performed for longer time; the average rate of the exchange performed for 1 day at 55℃ is 5.6 mol%, when the reaction was performed for 3 days this rate increased to 13.1 mol%, this rate increased to 43.5 mol% when the reaction time was extended to 6 days. It has to be mentioned that the value for the 6 day exchange is only based on 2 samples, but the minimum value for this method (32.4 mol%) still is slightly bigger than the maximum value for the 3 day exchange (32.3 mol%). Increasing the temperature of the reaction also resulted in higher manganese rates. The exchange reaction for two weeks at room temperature resulted in an average rate of 11.8 mol%, with the reaction performed at 55℃ only 3 days are needed to obtain an average rate of 13.1 mol%.

The exchange performed on ZIF-8 synthesised in aqueous ammonia resulted in lower manganese rates compared to the rates obtained by the reaction performed with ZIF-8 synthesised in methanol. For ZIF-8 synthesised in aqueous ammonia

an average manganese rate of 1.6 mol% was obtained for the exchange reaction for 1 day at 55℃. Some typical exchange rates are shown in Table A.1.

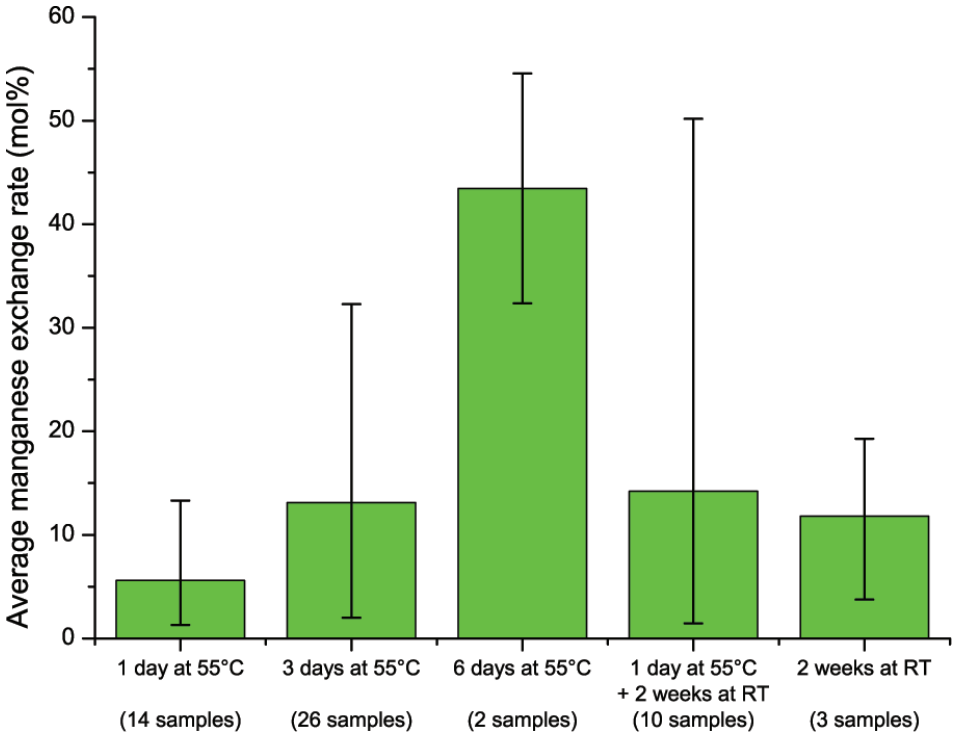


Figure 4.14: Average manganese rates obtained sorted on time and temperature used for the exchange reactions. The minimum and maximum value of the exchange rate for each method are shown by the bars.

The ZIF-8 particles exchanged with manganese were studied with SEM to see if the morphology of the particles has changed after the exchange. In Figure 4.15 SEM images of ZIF-8 synthesised in methanol (Figure 4.15a) and ZIF-8 exchanged with manganese (Figure 4.15b, c & d) are shown. The particles have a hexagonal shape and a smooth surface with an average size of 80 nm. Before and after the exchange reaction the particles look similar.

With energy-dispersive X-ray spectroscopy the Mn:Zn molar ratio was determined for two different samples. The results, compared with the Mn:Zn molar ratios measured using AAS, are shown in Table 4.1. As can be seen the values for the ratios measured with the two techniques are significantly different. AAS gave ratios of 50 and 32 mol%, for the same samples manganese rates of 35 and 28 mol%, respectively, were obtained with SEM-EDX. Since the X-rays for the SEM-EDX measurement slightly penetrates the sample two options are possible; the manganese content is either in the centre of the particles or it is located at the surface. Due to diffusion it is more likely that the manganese content is only

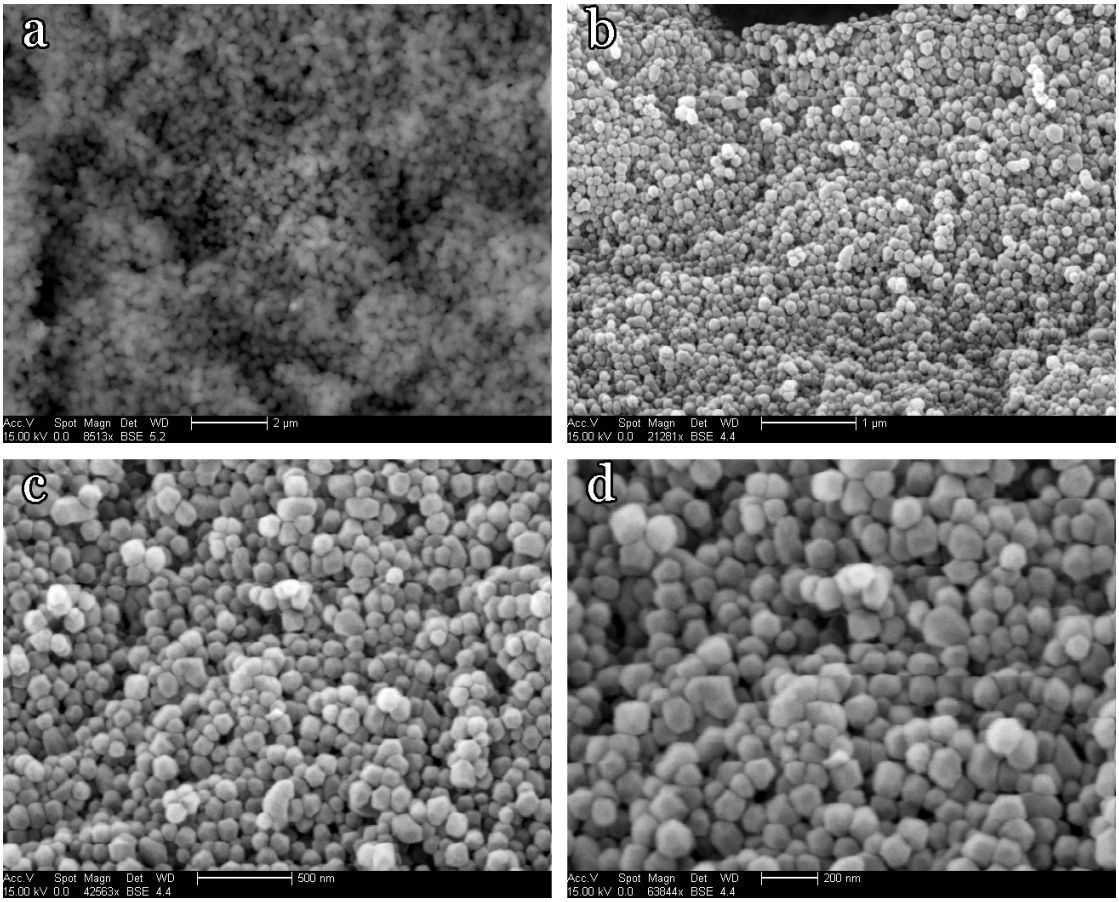


Figure 4.15: SEM images of ZIF-8 synthesised in methanol (a) and ZIF-8 exchanged with manganese shown at different magnifications (b, c & d). No visual differences are observed after the exchange reaction with manganese.

Table 4.1: Mn:Zn molar ratios measured with AAS compared with the ratios measured with SEM-EDX. The ratios measured with SEM-EDX are significantly lower than the rates measured with AAS. This indicates that the manganese is mostly located on the outside of the ZIF-8 crystals.

| Sample name | AAS (Mn:Zn mol%) | SEM-EDX (Mn:Zn mol%) |
|---|---|---|
| Mn[1] | 50 | 32 |
| Mn[2] | 35 | 28 |

located at the surface of the particles than that the manganese content is only present in the centre of the particles. To get more insight in the location of the manganese content Transmission Electron Microscopy (TEM) is used.

In Figure 4.16a & b TEM images of ZIF-8 synthesised in methanol are shown. Monodisperse hexagonally shaped particles with sharp edges are shown, the average particle size is 70 nm. The TEM images of the samples obtained after the exchange with manganese are shown in Figure 4.16c-f, the manganese content of the particles, determined with AAS, is 13 mol% (Figure 4.16c & d) and 18 mol% (Figure 4.16e & f). The ZIF-8 particles still looks similar in size and shape to the parent ZIF-8 particles. However, many small darker spots are visible which looks to be nanoparticles located on the surface of the ZIF-8 particles. To see if manganese is located inside of the ZIF-8 particles, and to analyse the chemical composition of the nanoparticles on the surface of the big particles, TEM-EDX measurements were performed. In Figure 4.17a an image is shown obtained using High-Angle Annular Dark Field TEM (HAADF-TEM). In the image two areas are shown, at the edge of a particle on which a nanoparticle is located (area 1) and at the centre of a particle on which no nanoparticles are visible (area 2). The results of the EDX measurements are presented in Figure 4.17b (area 1) & c (area 2). In the EDX spectrum obtained from the nanoparticle at the edge of the ZIF-8 particle the zinc concentration is low compared to the manganese concentration, but when looking at the spectrum obtained from the centre of the particle the manganese content is negligible. This indicates that the manganese is located only at the surface of the ZIF-8 particles and that it isn't incorporated into the framework.

Table 4.2: BET surface area and pore volume measured with $N_2$-physisorption, manganese molar rates are shown between brackets.

| **Sample name** | **BET surface area ($m^2g^{-1}$)** | **Pore volume ($cm^3g^{-1}$)** |
|---|---|---|
| ZIF-8 synthesised in methanol | 1818 | 0.85 |
| ZIF-8 synthesised in DMF | 982 | 0.28 |
| ZIF-8 exchanged with manganese [14%] | 1593 | 0.70 |
| ZIF-8 exchanged with manganese [50%] | 1136 | 0.48 |
| ZIF-8 exchanged with cobalt | 1365 | 0.60 |

The presence of adsorbed species on the surfaces and in the pores after the exchange reaction is confirmed by $N_2$-physisorption. In Table 4.2 physisorption data for both the parent ZIF-8 and ZIF-8 after the exchange reaction with manganese are shown. Before the exchange reaction ZIF-8 synthesised in methanol has a BET surface area of 1818 $m^2g^{-1}$ and a pore volume of 0.85 $cm^3g^{-1}$, after the reaction the surface area decreased to 1593 and 1136 $m^2g^{-1}$ with pore volumes of 0.70 and 0.48 $cm^3g^{-1}$ for samples with a manganese rate of 14 and 50 mol% respectively. This indicates that after the exchange reaction absorbed species are present in the pores of ZIF-8.

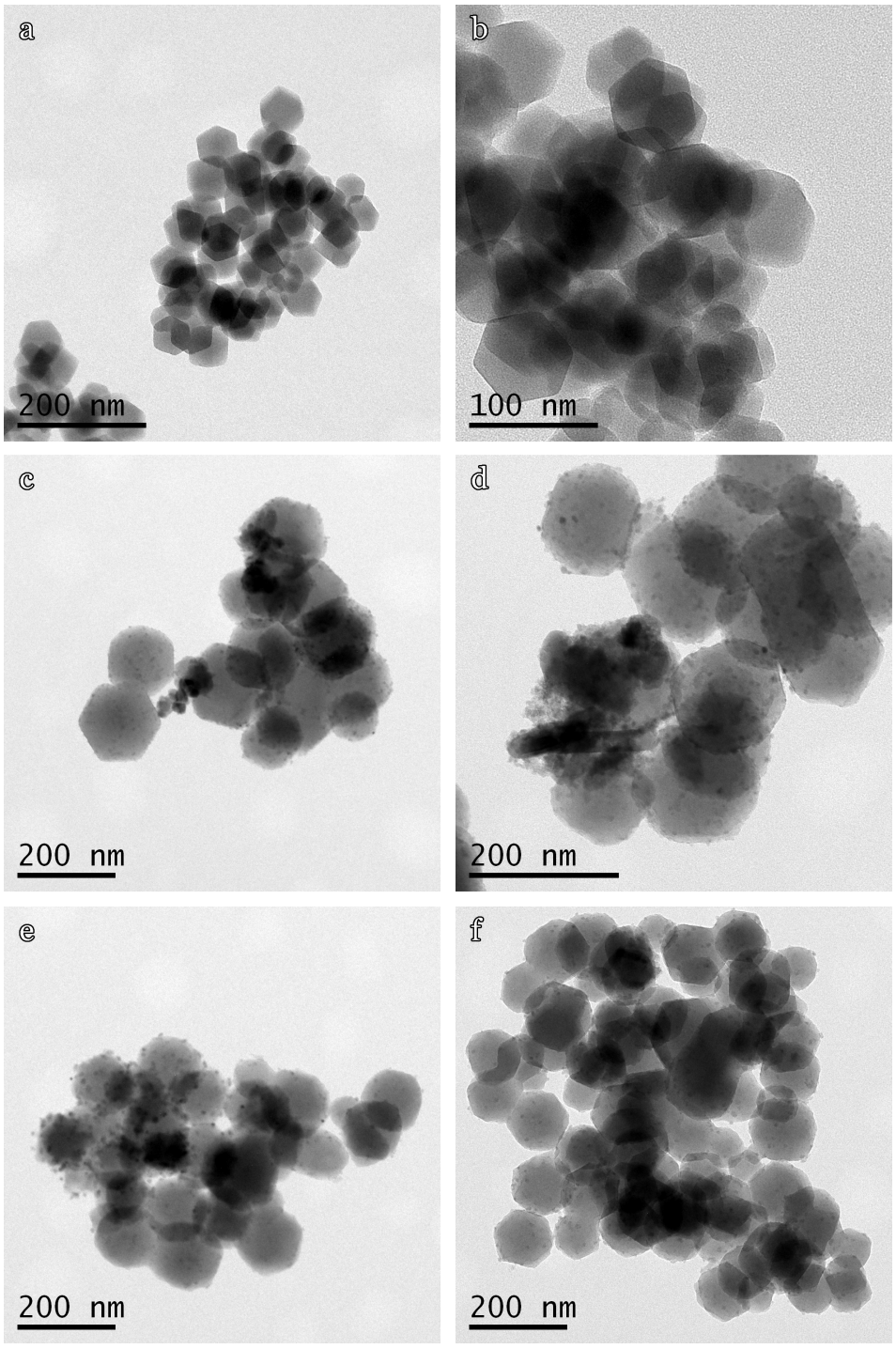


Figure 4.16: TEM images of pure ZIF-8 synthesised in methanol (a & b) and ZIF-8 after the exchange reaction with manganese for 1 day (c & d, 13 mol% manganese) and for 3 days (e & f, 18 mol% manganese), all performed at 55℃.

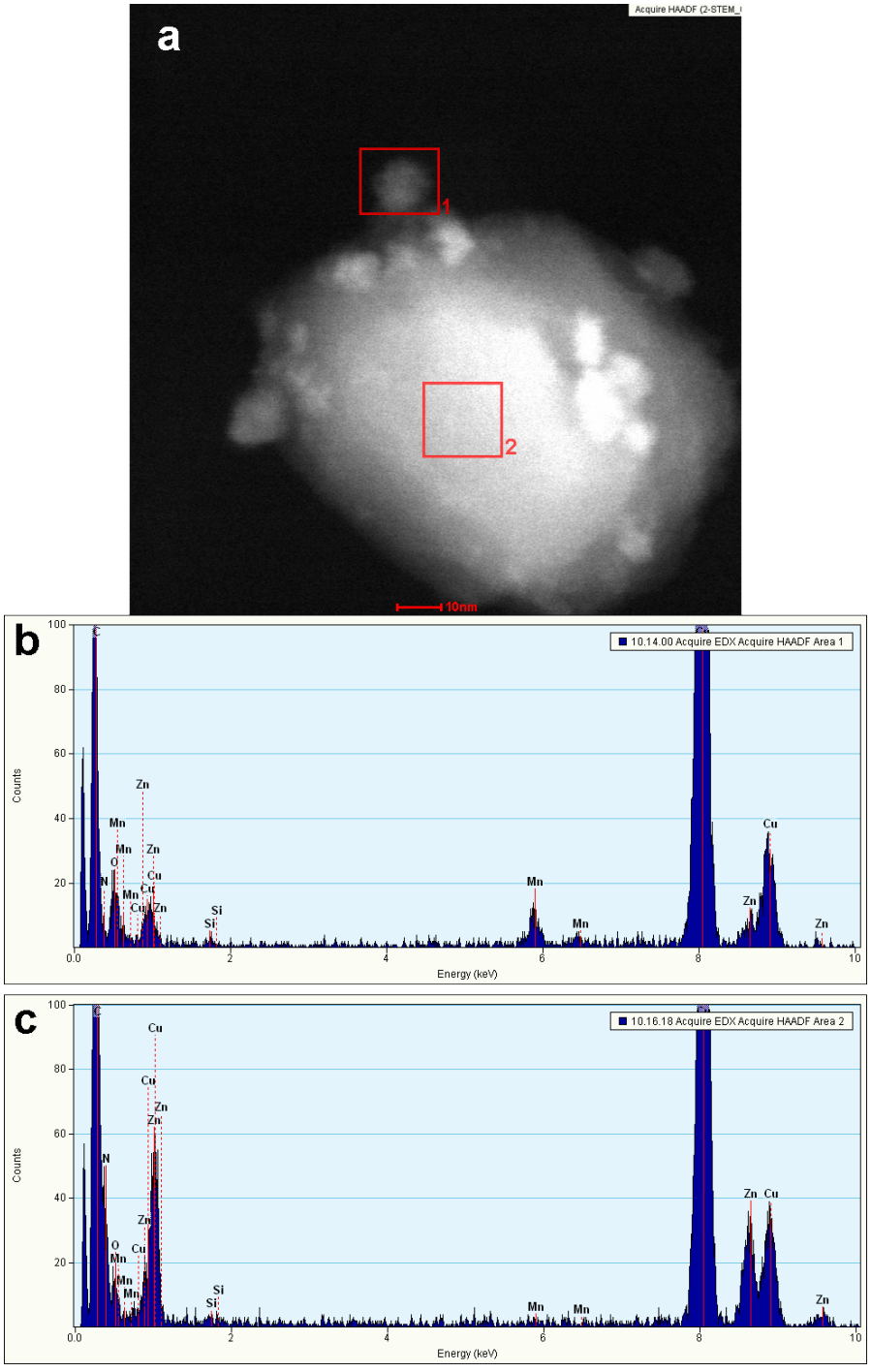


Figure 4.17: TEM images of ZIF-8 after the exchange reaction with manganese for 3 days. Two squares are shown where EDX measurements were performed (results of square 1 are shown in figure b, square 2 is shown in Figure c).

# 5 Conclusions

ZIF-8 was successfully synthesised using different methods as described in section 3.1. All methods resulted in white ZIF-8 crystals which crystal structure was confirmed with use of X-ray diffraction. Infrared spectroscopy showed that all of the 2-methylimidazole linker has been deprotonated during the reaction or was removed during the purification of the product. Some differences were observed, the drying process for the ZIF-8 crystals synthesised in DMF didn't result in complete empty pores as seen in the IR spectrum in which bands of DMF are present. From this can be concluded that emerging the crystals in methanol for 3 days is not sufficient to fully exchange the DMF from the pores with methanol, which probably is due to the coordination of DMF to the framework. The different synthesis methods resulted in different shapes and crystal sizes as seen with SEM, the synthesis in DMF at 140℃ resulted in the biggest particles with a size of ± 100-200 µm on which smaller particles were observed. Cubic shaped particles with an average size of 700 nm with smooth surfaces were obtained using aqueous ammonia as reaction medium at room temperature. With methanol as solvent at 55℃ crystal sizes of ± 80 nm were obtained which are hexagonally shaped with smooth surfaces.

To see if it is possible to directly synthesise ZIF-8 with manganese incorporated in the framework ZIF-8 was synthesised in the presence of manganese(II) ions. Although both XRD and FTIR confirmed that the ZIF-8 structure was obtained by this synthesis, AAS results showed that manganese wasn't present in the final product. So it is not possible to synthesise ZIF-8(Zn/Mn) directly by solvothermal synthesis in DMF and post-synthetic modification is needed to obtain ZIF-8 with manganese(II) incorporated in the framework.

To obtain ZIF-8 with other metal-ions incorporated in the framework, cation exchange using different metal-ions was performed. The metal-ion exchange with copper wasn't successful as it disturbed the ZIF-8 framework, which is shown by the diffractograms in Figure 4.8. The crystal structure of ZIF-8 was retained after the exchange reaction with cobalt(II) and manganese(II). The infrared spectra showed the same spectral features as observed in the spectrum of the parent ZIF-8. The thermal stability of ZIF-8 after the exchange reaction was slightly lower compared to the parent ZIF-8 (577℃ compared to 587℃), but no changes in crystal structure were observed in the diffractogram measured while heating up to 500℃.

Different parameters for the exchange reaction were tested. The optimal pH for the metal-ion exchange in ZIF-8 was found with pH∼7, as a higher pH leads to the formation of metal oxides and metal hydroxides and in acidic medium the 2-methylimidazolate linker is protonated leading to the dissolution of ZIF-8 until pH∼7 is reached. Similar results for the exchange rates were observed when the exchange reaction was performed in methanol and DMF. Exchange rates

when water was used as solvent could not be obtained as the product couldn't be dissolved in nitric acid. This indicates that metal oxide or metal hydroxide species were formed during this reaction instead of incorporation of metal-ions in the ZIF-8 framework. The exchange reaction with cobalt(II) and the reactions performed under inert conditions gave negligible metal rates For the metal-ion exchange with manganese a wide range of manganese rates was observed when the same parameters were used. It still could be concluded that both temperature and time had a positive effect on the manganese rate that was obtained after the exchange reaction. The lowest average manganese rates were obtained for the exchange reaction of 1 day at 55℃ with an average manganese rate of 5.6 mol%. The highest average manganese rate was obtained for the exchange reaction for 6 days at 55℃ with an average of 43.5 mol%. When looking at the SEM images of ZIF-8 before and after metal-ion exchange the particles looks similar in size and shape, but when the manganese rates were determined using SEM-EDX significantly lower values were obtained compared to the AAS results, which indicated that the manganese was mostly located on the surface of the crystals.

For more insight in the location of the manganese content TEM was used. TEM-EDX confirmed that manganese nanoparticles were located only at the surface of the crystals and did not incorporate into the ZIF-8 framework. The adsorption of manganese content was also shown by $N_2$-physisorption measurements with the decrease of both the BET surface area (from 1818 to 1136 $m^2g^{-1}$) and pore volume (from 0.85 to 0.48 $cm^3g^{-1}$) after the exchange reaction.

# 6 Outlook

**ZIF-8 synthesis**
ZIF-8 can be synthesised using different techniques to see the effect on the size and shape. This might lead to a better candidate for the metal-ion exchange. Also particles with different crystal sizes can be synthesised by varying the reaction time. A shorter reaction time will lead to a decrease in particle size.

**Post-synthetic modification**
The pores of the ZIF-8 framework are poorly accessible because of the small pore aperture of ZIF-8 (3.4 Å). This might prevent the metal precursor to enter the pores of the framework and perform metal-ion exchange at the inner surface of the material. The pore aperture can be increased by solvent-assisted linker exchange of 2-methylimidazole by imidazole. This exchange can lead to a pore aperture of at least 6.1 Å[102] which makes it easier for molecules to enter the pores of the framework.

Since it is likely that manganese oxide/hydroxide nanoparticles were formed during the reaction, the exchange reaction performed under inert conditions has to be further investigated. Until now it gave negligible exchange rates, but with the use of different solvents (for example DMF), higher concentrations for the manganese precursor, higher temperatures or longer reaction times it might be possible to obtain significant exchange rates.

For the concept of metal-ion exchange, more exchanges with cobalt can be performed. Cation exchange with cobalt should be possible, as there is an isostructural variant of ZIF-8 with cobalt(II) instead of zinc(II) as metal-ions (ZIF-67). This can give more insight in the exchange reaction to see which parameters have a positive influence on the metal-ion exchange.

**Analysis**
X-ray photoelectron spectroscopy (XPS) analysis can be useful to get information about the kind of manganese to get information about the manganese species on the surface of the particles. Also scanning transmission electron microscopy combines with electron energy loss spectroscopy (STEM-EELS) can be an useful technique to see in which chemical environment the manganese species are present, it might also be used to determine which metal−nitrogen bonds are present in the samples.

**Catalysis**
When metal-ion exchange has been performed successfully on ZIF-8, catalysis can be performed to see if a higher catalytic activity is obtained compared to the

parent ZIF-8. Possible reactions reported in literature in which manganese is used as catalyst are the oxidation of an alcohol or the epoxidation of an olefin.

# Bibliography


[1] A. Phan, C. J. Doonan, F. J. Uribe-Romo, C. B. Knobler, M. O'Keeffe, and O. M. Yaghi, "Synthesis, Structure, and Carbon Dioxide Capture Properties of Zeolitic Imidazolate Frameworks," *Acc. Chem. Res.*, vol. 43, no. 1, pp. 58–67, 2010.

[2] K. S. Park, Z. Ni, A. P. Côté, J. Y. Choi, R. Huang, F. J. Uribe-Romo, H. K. Chae, M. O'Keeffe, and O. M. Yaghi, "Exceptional Chemical and Thermal Stability of Zeolitic Imidazolate Frameworks," *Proc. Natl. Acad. Sci.*, vol. 103, no. 27, pp. 10 186–10 191, 2006.

[3] C. Janiak and J. K. Vieth, "MOFs, MILs and more: Concepts, Properties and Applications for Porous Coordination Networks (PCNs)," *New J. Chem.*, vol. 34, no. 11, pp. 2366–2388, 2010.

[4] J. Lee, O. K. Farha, J. Roberts, K. A. Scheidt, S. T. Nguyen, and J. T. Hupp, "Metal-Organic Framework Materials as Catalysts," *Chem. Soc. Rev.*, vol. 38, no. 5, pp. 1450–1459, 2009.

[5] A. Primo and H. Garcia, "Zeolites as Catalysts in Oil Refining," *Chem. Soc. Rev.*, vol. 43, pp. 7548–7561, 2014.

[6] C. Baerlocher, "Database of Zeolite Structures," Apr. 2015. [Online]. Available: http://www.iza-structure.org/databases/

[7] J. García-Martínez, M. Johnson, J. Valla, K. Li, and J. Y. Ying, "Mesostructured Zeolite Y - High Hydrothermal Stability and Superior FCC Catalytic Performance," *Catal. Sci. Technol.*, vol. 2, pp. 987–994, 2012.

[8] K. Kubo, H. Iida, S. Namba, and A. Igarashi, "Comparison of steaming stability of Cu-ZSM-5 with those of Ag-ZSM-5, P/H-ZSM-5, and H-ZSM-5 zeolites as naphtha cracking catalysts to produce light olefin at high temperatures," *Appl. Catal. A*, vol. 489, pp. 272–279, 2015.

[9] S. Kitagawa, R. Kitaura, and S.-I. Noro, "Functional porous coordination polymers," *Angew. Chem. Int. Ed.*, vol. 43, pp. 2334–2375, 2004.

[10] D. Farrusseng, S. Aguado, and C. Pinel, "Metal-Organic frameworks: Opportunities for Catalysis," *Angew. Chem. Int. Ed.*, vol. 48, no. 41, pp. 7502–7513, 2009.

[11] C.-T. Chen and K. S. Suslick, "One-dimensional coordination polymers: Applications to material science," *Coord. Chem. Rev.*, vol. 128, pp. 293–322, 1993.

[12] M. Ranocchiari and J. A. van Bokhoven, "Catalysis by metal-organic frameworks: fundamentals and opportunities." *Phys. Chem. Chem. Phys.*, vol. 13, no. 14, pp. 6388–6396, 2011.

[13] N. Stock and S. Biswas, "Synthesis of Metal-Organic Frameworks (MOFs): Routes to Various MOF Topologies, Morphologies, and Composites," *Chem. Rev.*, vol. 112, pp. 933–969, 2012.

[14] O. M. Yaghi and H. Li, "Hydrothermal Synthesis of a Metal-Organic Framework Containing Large Rectangular Channels," *J. Am. Chem. Soc.*, vol. 117, no. 41, pp. 10 401–10 402, 1995.

[15] O. K. Farha, I. Eryazici, N. C. Jeong, B. G. Hauser, C. E. Wilmer, A. A. Sarjeant, R. Q. Snurr, S. T. Nguyen, A. O. Yazaydin, and J. T. Hupp, "Metal-Organic Framework Materials with Ultrahigh Surface Areas: Is the Sky the Limit?" *J. Am. Chem. Soc.*, vol. 134, no. 36, pp. 15 016–15 021, 2012.

[16] S. Qiu and G. Zhu, "Molecular engineering for synthesizing novel structures of metal-organic frameworks with multifunctional properties," *Coord. Chem. Rev.*, vol. 253, no. 23-24, pp. 2891–2911, 2009.

[17] C. Dey, T. Kundu, B. P. Biswal, A. Mallick, and R. Banerjee, "Crystalline metal-organic frameworks (MOFs): synthesis, structure and function," *Acta Cryst.*, vol. B70, pp. 3–10, 2014.

[18] M. Eddaoudi, D. F. Sava, J. F. Eubank, K. Adil, and V. Guillerm, "Zeolite-like metalorganic frameworks (ZMOFs): design, synthesis, and properties," *Chem. Soc. Rev.*, vol. 44, pp. 228–249, 2015.

[19] P. Barbosa, N. C. Rosero-Navarro, F.-N. Shi, and F. M. Figueiredo, "Protonic Conductivity of Nanocrystalline Zeolitic Imidazolate Framework 8," *Electrochim. Acta*, vol. 153, pp. 19–27, 2015.

[20] B. Chen, Z. Yang, Y. Zhu, and Y. Xia, "Zeolitic imidazolate framework materials: recent progress in synthesis and applications," *J. Mater. Chem. A*, vol. 2, no. 40, pp. 16 811–16 831, 2014.

[21] Y.-N. Wu, M. Zhou, B. Zhang, B. Wu, J. Li, J. Qiao, X. Guan, and F. Li, "Amino acid assisted templating synthesis of hierarchical zeolitic imidazolate framework-8 for efficient arsenate removal." *Nanoscale*, vol. 6, no. 2, pp. 1105–1112, 2013.

[22] A. U. Czaja, N. Trukhan, and U. Müller, "Industrial applications of metal-organic frameworks." *Chem. Soc. Rev.*, vol. 38, no. 5, pp. 1284–1293, 2009.

[23] H. Fei, J. F. Cahill, K. A. Prather, and S. M. Cohen, "Tandem Postsynthetic Metal on and Ligand Exchange in Zeolitic Imidazolate Frameworks," *Inorg. Chem.*, vol. 52, no. 7, pp. 4011–4016, 2013.

[24] S. R. Venna, J. B. Jasinski, and M. A. Carreon, "Structural Evolution of Zeolitic Imidazolate Framework-8," *J. Am. Chem. Soc.*, vol. 132, no. 51, pp. 18 030–18 033, 2010.

[25] Y.-T. Liao, S. Dutta, C.-H. Chien, C.-C. Hu, F.-K. Shieh, C.-H. Lin, and K. C.-W. Wu, "Synthesis of Mixed-Ligand Zeolitic Imidazolate Framework (ZIF-8-90) for $CO_2$ Adsorption," *J. Inorg. Organomet. Polym.*, vol. 25, pp. 251–258, 2015.

[26] N. Keser Demir, B. Topuz, L. Yilmaz, and H. Kalipcilar, "Synthesis of ZIF-8 from recycled mother liquors," *Microporous Mesoporous Mater.*, vol. 198, pp. 291–300, 2014.

[27] J. Zakzeski, A. Dbczak, P. C. A. Bruijnincx, and B. M. Weckhuysen, "Catalytic oxidation of aromatic oxygenates by the heterogeneous catalyst Co-ZIF-9," *Appl. Catal. A*, vol. 394, no. 1-2, pp. 79–85, 2011.

[28] S. Bhattacharjee, M.-S. Jang, H. I. Kwon, and W.-S. Ahn, "Zeolitic Imidazolate Frameworks: Synthesis, Functionalization, and Catalytic/Adsorption Applications," *Chem. Surv. Asia*, vol. 18, no. 4, pp. 101–127, 2014.

[29] Y. Hu, Z. Liu, J. Xu, Y. Huang, and Y. Song, "Evidence of pressure enhanced CO2 storage in ZIF-8 probed by FTIR spectroscopy." *J. Am. Chem. Soc.*, vol. 135, no. 25, pp. 9287–90, Jun. 2013. [Online]. Available: http://www.ncbi.nlm.nih.gov/pubmed/23758491

[30] M. Zhu, D. Srinivas, S. Bhogeswararao, P. Ratnasamy, and M. A. Carreon, "Catalytic activity of ZIF-8 in the synthesis of styrene carbonate from $CO_2$ and styrene oxide," *Catal. Commun.*, vol. 32, no. 3, pp. 36–40, 2013.

[31] J.-S. Qin, D.-Y. Du, W.-L. Li, J.-P. Zhang, S.-L. Li, Z.-M. Su, X.-L. Wang, Q. Xu, K.-Z. Shao, and Y.-Q. Lan, "N-rich zeolite-like metalorganic framework with sodalite topology: high CO2 uptake, selective gas adsorption and efficient drug delivery," *Chem. Sci.*, vol. 3, no. 6, p. 2114, 2012. [Online]. Available: http://xlink.rsc.org/?DOI=c2sc00017b

[32] S. Takaishi, E. J. DeMarco, M. J. Pellin, O. K. Farha, and J. T. Hupp, "Solvent-assisted linker exchange (SALE) and post-assembly metallation in porphyrinic metal-organic framework materials," *Chem. Sci.*, vol. 4, pp. 1509–1513, 2013.

[33] O. Karagiaridi, W. Bury, J. E. Mondloch, J. T. Hupp, and O. K. Farha, "Solvent-Assisted Linker Exchange: An Alternative to the De Novo Synthesis of Unattainable Metal-Organic Frameworks," *Angew. Chem. Int. Ed.*, vol. 53, pp. 4530–4540, 2014.

[34] J. D. Evans, C. J. Sumby, and C. J. Doonan, "Post-synthetic metalation of metalorganic frameworks," *Chem. Soc. Rev.*, vol. 43, pp. 5933–5951, 2014.

[35] W. Lu, Z. Wei, Z.-Y. Gu, T.-F. Liu, J. Park, J. Park, J. Tian, M. Zhang, Q. Zhang, T. Gentle III, M. Bosch, and H.-C. Zhou, "Tuning the structure and function of metal-organic frameworks via linker design," *Chem. Soc. Rev.*, vol. 43, pp. 5561–5593, 2014.

[36] C.-P. Li and M. Du, "Role of solvents in coordination supramolecular systems," *Chem. Commun.*, vol. 47, no. 21, pp. 5958–5972, 2011.

[37] E. L. Bustamante, J. L. Fernández, and J. M. Zamaro, "Influence of the solvent in the synthesis of zeolitic imidazolate framework-8 (ZIF-8) nanocrystals at room temperature," *J. Colloid Interface Sci.*, vol. 424, pp. 37–43, 2014.

[38] H.-C. J. Zhou and S. Kitagawa, "Metal-Organic Frameworks (MOFs)," *Chem. Soc. Rev.*, vol. 43, pp. 5415–5418, 2014.

[39] R. Banerjee, A. Phan, B. Wang, C. Knobler, H. Furukawa, M. O'Keeffe, and O. M. Yaghi, "High-Throughput Synthesis of Zeolitic Imidazolate Frameworks and Application to $CO_2$ Capture," *Science (80-. ).*, vol. 319, no. 5865, pp. 939–943, 2008.

[40] Z.-J. Lin, J. Lü, M. Hong, and R. Cao, "Metal-organic frameworks based on flexible ligands (FL-MOFs): structures and applications," *Chem. Soc. Rev.*, vol. 43, pp. 5867–5895, 2014.

[41] M. Eddaoudi, J. Kim, N. Rosi, D. Vodak, J. Wachter, M. O'Keeffe, and O. M. Yaghi, "Systematic Design of Pore Size and Functionality in Isoreticular MOFs and Their Application in Methane Storage." *Science (80-. ).*, vol. 295, no. 5554, pp. 469–472, 2002.

[42] M. Fujita and Y. Kwon, "Preparation, Clathration Ability, and Catalysis of a Two-Dimensional Square Network Material Composed of Cadmium(II)

and 4,4'-Bipyridine," *J. Am. Chem. Soc.*, vol. 116, no. 1 3, pp. 1151–1152, 1994.

[43] P. Horcajada, S. Surblé, C. Serre, D.-Y. Hong, Y.-K. Seo, J.-S. Chang, J.-M. Grenèche, I. Margiolaki, and G. Férey, "Synthesis and catalytic properties of MIL-100(Fe), an iron(III) carboxylate with large pores." *Chem. Commun.*, vol. 100, no. 27, pp. 2820–2822, 2007.

[44] N. V. Maksimchuk, K. A. Kovalenko, S. S. Arzumanov, Y. A. Chesalov, M. S. Melgunov, A. G. Stepanov, V. P. Fedin, and O. A. Kholdeeva, "Hybrid polyoxotungstate/MIL-101 materials: Synthesis, characterization, and catalysis of $H_2O_2$-based alkene epoxidation," *Inorg. Chem.*, vol. 49, no. 6, pp. 2920–2930, 2010.

[45] S. C. Jones and C. A. Bauer, "Diastereoselective heterogeneous bromination of stilbene in a porous metal-organic framework," *J. Am. Chem. Soc.*, vol. 131, no. 35, pp. 12 516–12 517, 2009.

[46] M. Sabo, A. Henschel, H. Fröde, E. Klemm, and S. Kaskel, "Solution infiltration of palladium into MOF-5: synthesis, physisorption and catalytic properties," *J. Mater. Chem.*, vol. 17, pp. 3827–3832, 2007.

[47] B. Chen, F. Bai, Y. Zhu, and Y. Xia, "A cost-effective method for the synthesis of zeolitic imidazolate framework-8 materials from stoichiometric precursors via aqueous ammonia modulation at room temperature," *Microporous Mesoporous Mater.*, vol. 193, pp. 7–14, 2014.

[48] J. Cravillon, S. Münzer, S.-J. Lohmeier, A. Feldhoff, K. Huber, and M. Wiebcke, "Rapid Room-Temperature Synthesis and Characterization of Nanocrystals of a Prototypical Zeolitic Imidazolate Framework," *Chem. Mater.*, vol. 21, no. 8, pp. 1410–1412, 2009.

[49] S. Tanaka, K. Kida, M. Okita, Y. Ito, and Y. Miyake, "Size-controlled Synthesis of Zeolitic Imidazolate Framework-8 (ZIF-8) Crystals in an Aqueous System at Room Temperature," *Chem. Lett.*, vol. 41, pp. 1337–1339, 2012.

[50] M. Zhu, S. R. Venna, J. B. Jasinski, and M. A. Carreon, "Room-Temperature Synthesis of ZIF-8: The Coexistence of ZnO Nanoneedles," *Chem. Mater.*, vol. 23, pp. 3590–3592, 2011.

[51] D. Peralta, G. Chaplais, A. Simon-Masseron, K. Barthelet, and G. D. Pirngruber, "Synthesis and adsorption properties of ZIF-76 isomorphs," *Microporous Mesoporous Mater.*, vol. 153, pp. 1–7, 2012.

[52] J. Cravillon, R. Nayuk, S. Springer, A. Feldhoff, K. Huber, and M. Wiebcke, "Controlling Zeolitic Imidazolate Framework Nano- and Microcrystal Formation: Insight into Crystal Growth by Time-Resolved In Situ Static Light Scattering," *Chem. Mater.*, vol. 23, pp. 2130–2141, 2011.

[53] S. K. Nune, P. K. Thallapally, A. Dohnalkova, C. Wang, J. Liu, and G. J. Exarhos, "Synthesis and properties of nano zeolitic imidazolate frameworks," *Chem. Commun.*, vol. 46, pp. 4878–4880, 2010.

[54] T. Ahnfeldt, N. Guillou, D. Gunzelmann, I. Margiolaki, T. Loiseau, G. Férey, J. Senker, and N. Stock, "$[Al_4(OH)_2(OCH_3)_4(H_2N\text{-}bdc)_3]\cdot xH_2O$: A 12-Connected Porous Metal-Organic Framework with an Unprecedented Aluminum-Containing Brick," *Angew. Chem. Int. Ed.*, vol. 48, pp. 5163–5166, 2009.

[55] H. L. Jiang, Y. Tatsu, Z. H. Lu, and Q. Xu, "Non-, Micro-, and Mesoporous Metal-Organic Framework Isomers: Reversible Transformation, Fluorescence Sensing, and Large Molecule Separation," *J. Am. Chem. Soc.*, vol. 132, pp. 5586–5587, 2010.

[56] L. Luo, K. Chen, Q. Liu, Y. Lu, T. A. Okamura, G. C. Lv, Y. Zhao, and W. Y. Sun, "Zinc(II) and Cadmium(II) Complexes with 1,3,5-Benzenetricarboxylate and Imidazole-Containing Ligands: Structural Variation via Reaction Temperature and Solvent," *Cryst. Growth Des.*, vol. 13, pp. 2312–2321, 2013.

[57] A. Schneemann, V. Bon, I. Schwedler, I. Senkovska, S. Kaskel, and R. A. Fischer, "Flexible metal-organic frameworks," *Chem. Soc. Rev.*, vol. 43, pp. 6062–6096, 2014.

[58] Y.-X. Sun and W.-Y. Sun, "Influence of temperature on metal-organic frameworks," *Chin. Chem. Lett.*, vol. 25, pp. 823–828, 2014.

[59] G.-X. Liu, H. Xu, H. Zhou, S. Nishihara, and X.-M. Ren, "Temperature-induced assembly of MOF polymorphs: Syntheses, structures and physical properties," *CrystEngComm*, vol. 14, pp. 1856–1864, 2012.

[60] L. T. L. Nguyen, K. K. A. Le, and N. T. S. Phan, "A Zeolite Imidazolate Framework ZIF-8 Catalyst for Friedel-Crafts Acylation," *Chin. J. Catal.*, vol. 33, no. 4, pp. 688–696, 2012.

[61] Y.-R. Lee, J. Kim, and W.-S. Ahn, "Synthesis of metal-organic frameworks: A mini review," *Korean J. Chem. Eng.*, vol. 30, no. 9, pp. 1667–1680, 2013.

[62] M. He, J. Yao, Q. Liu, K. Wang, F. Chen, and H. Wang, "Facile synthesis of zeolitic imidazolate framework-8 from a concentrated aqueous solution," *Microporous Mesoporous Mater.*, vol. 184, pp. 55–60, 2014.

[63] Y. Pan, Y. Liu, G. Zeng, L. Zhao, and Z. Lai, "Rapid synthesis of zeolitic imidazolate framework-8 (ZIF-8) nanocrystals in an aqueous system," *Chem. Commun.*, vol. 47, no. 7, pp. 2071–2073, 2011.

[64] A. F. Gross, E. Sherman, and J. J. Vajo, "Aqueous room temperature synthesis of cobalt and zinc sodalite zeolitic imidizolate frameworks," pp. 5458–5460, 2012.

[65] J. Yao, M. He, K. Wang, R. Chen, Z. Zhong, and H. Wang, "High-yield synthesis of zeolitic imidazolate frameworks from stoichiometric metal and ligand precursor aqueous solutions at room temperature," *CrystEngComm*, vol. 15, pp. 3601–3606, 2013.

[66] S. T. Meek, J. a. Greathouse, and M. D. Allendorf, "Metal-Organic Frameworks: A Rapidly Growing Class of Versitile Nanoporous Materials," *Adv. Mater.*, vol. 23, no. 2, pp. 249–267, 2011.

[67] A. M. Joaristi, J. Juan-Alcañiz, P. Serra-Crespo, F. Kapteijn, and J. Gascon, "Electrochemical Synthesis of Some Archetypical $Zn^{2+}$, $Cu^{2+}$, and $Al^{3+}$ Metal Organic Frameworks," *Gryst. Growth. Des.*, vol. 12, pp. 3489–3498, 2012.

[68] M. Klimakow, P. Klobes, K. Rademann, and F. Emmerling, "Characterization of mechanochemically synthesized MOFs," *Microporous Mesoporous Mater.*, vol. 154, pp. 113–118, 2012.

[69] D. C. Harris, "Quantitative Chemical Analysis," in *Quant. Chem. Anal.*, 8th ed. New York: W. H. Freeman and Company, 2010, pp. 565–595, 705.

[70] D. Farrusseng, J. Canivet, and A. Quadrelli, *Design of Functional Metal Organic Frameworks by Post-Synthetic Modification*, 1st ed., D. Farrusseng, Ed. Wiley-VCH Verlag GmbH & Co. KGaA., 2011.

[71] Z. Wang and S. M. Cohen, "Postsynthetic modification of metal-organic frameworks," *Chem. Soc. Rev.*, vol. 38, no. 5, pp. 1315–1329, 2009.

[72] P. Deria, J. E. Mondloch, O. Karagiaridi, W. Bury, J. T. Hupp, and O. K. Farha, "Beyond post-synthesis modification: evolution of metal-organic frameworks via building block replacement," *Chem. Soc. Rev.*, vol. 43, pp. 5896–5912, 2014.

[73] S. M. Cohen, "Modifying MOFs: new chemistry, new materials," *Chem. Sci.*, vol. 1, no. 1, pp. 32–36, 2010.

[74] H. Fei, J. Shin, Y. S. Meng, M. Adelhardt, J. Sutter, K. Meyer, and S. M. Cohen, "Reusable Oxidation Cataysis Using Metal-Monocatecholato Species in a Robust Metal-Organic Framework," *J. Am. Chem. Soc.*, vol. 136, no. 13, pp. 4965–4973, 2014.

[75] S. M. Cohen, "Postsynthetic Methods for the Functionalization of Metal-Organic Frameworks," *Chem. Rev.*, vol. 112, no. 2, pp. 970–1000, 2012.

[76] Z. Wang, K. K. Tanabe, and S. M. Cohen, "Accessing Postsynthetic Modification in a Series of Metal-Organic Frameworks and the Influence of Framework Topology on Reactivity," *Inorg. Chem.*, vol. 48, no. 1, pp. 296–306, 2009.

[77] M. Banerjee, S. Das, M. Yoon, J. C. Hee, H. H. Myung, S. M. Park, G. Seo, and K. Kim, "Postsynthetic Modification Switches an Achiral Framework to Catalytically Active Homochiral Metal-Organic Porous Materials," *J. Am. Chem. Soc.*, vol. 131, pp. 7524–7525, 2009.

[78] T. Yamada and H. Kitagawa, "Protection and Deprotection Approach for the Introduction of Functional Groups into Metal-Organic Frameworks," *J. Am. Chem. Soc.*, vol. 131, pp. 6312–6313, 2009.

[79] M. Kim, J. F. Cahill, H. Fei, K. A. Prather, and S. M. Cohen, "Postsynthetic Ligand and Cation Exchange in Robust Metal-Organic Frameworks," *J. Am. Chem. Soc.*, vol. 134, no. 43, pp. 18 082–18 088, 2012.

[80] S. Das, H. Kim, and K. Kim, "Metathesis in Single Crystal: Complete and Reversible Exchange of Metal Ions Constituting the Frameworks of Metal-Organic Frameworks," *J. Am. Chem. Soc.*, vol. 131, no. 11, pp. 3814–3815, 2009.

[81] B. J. Burnett, P. M. Barron, C. Hu, and W. Choe, "Stepwise Synthesis of Metal-Organic Frameworks: Replacement of Structural Organic Linkers," *J. Am. Chem. Soc.*, vol. 133, no. 26, pp. 9984–9987, 2011.

[82] M. Kim, J. F. Cahill, Y. Su, K. A. Prather, and S. M. Cohen, "Postsynthetic ligand exchange as a route to functionalization of inert metalorganic frameworks," *Chem. Sci.*, vol. 3, no. 1, pp. 126–130, 2012.

[83] T. Li, M. T. Kozlowski, E. A. Doud, M. N. Blakely, and N. L. Rosi, "Stepwise Ligand Exchange for the Preparation of a Family of Mesoporous MOFs," *J. Am. Chem. Soc.*, vol. 135, pp. 11 688–11 691, 2013.

[84] A. F. Gross, E. Sherman, S. L. Mahoney, and J. J. Vajo, "Reversible Ligand Exchange in a Metal-Organic Framework (MOF): Toward MOF-Based Dynamic Combinatorial Chemical Systems," *J. Phys. Chem. A*, vol. 117, pp. 3771–3776, 2013.

[85] C. K. Brozek, L. Bellarosa, T. Soejima, T. V. Clark, N. Lõpez, and M. Dinc, "Solvent-Dependent Cation Exchange in Metal-Organic Frameworks," *Chem. Eur. J.*, vol. 20, no. 23, pp. 6871–6874, 2014.

[86] X. Song, T. K. Kim, H. Kim, D. Kim, S. Jeong, H. R. Moon, and M. S. Lah, "Post-Synthetic Modification of Framework Metal Ions in Isostructural Metal-Organic Frameworks: Core-Shell Heterostructures via Selective Transmetalations," *Chem. Mater.*, vol. 24, pp. 3065–3073, 2012.

[87] M. Lalonde, W. Bury, O. Karagiaridi, Z. Brown, J. T. Hupp, and O. K. Farha, "Transmetalation: routes to metal exchange within metalorganic frameworks," *J. Mater. Chem. A*, vol. 1, no. 18, pp. 5453–5468, 2013.

[88] H. Irving and R. J. P. Williams, "The Stability of Transition-metal Complexes," *J. Chem. Soc.*, pp. 3192–3210, 1953.

[89] M. Mhamdi, S. Khaddar-Zine, and A. Ghorbel, "Influence of the cobalt salt precursors on the cobalt speciation and catalytic properties of H-ZSM-5 modified with cobalt by solid-state ion exchange reaction," *Appl. Catal. A*, vol. 357, no. 1, pp. 42–50, 2009.

[90] PerkinElmer, "FT-IR Spectroscopy Attenuated Total Reflectance (ATR)," Feb. 2015. [Online]. Available: http://www.utsc.utoronto.ca/~traceslab/ATR_FTIR.pdf

[91] O. L. J. Gijzeman, *Adsorption, Adsorption Isotherms and Surface Texture*. Utrecht: Debye Institure - Inorganic Chemistry, Utrecht University, 2004.

[92] A. W. Coats and J. P. Redfern, "Thermogravimetric Analysis," *Analyst*, vol. 88, pp. 906–924, 1963.

[93] A. Technologies, "Atomic Absorption Spectroscopy," Apr. 2015. [Online]. Available: http://www.agilent.com/labs/features/2011_101_spectroscopy.html

[94] M. A. van Huis and H. Friedrich, "Electron Microscopy Techniques," in *Nanoparticles*, C. de Mello Donegá, Ed. Utrecht: Springer Berlin Heidelberg, 2014, ch. 7, pp. 191–219.

[95] B. Hachua, M. Nowak, and J. Kusz, "Crystal and Molecular Structure Analysis of 2-Methylimidazole," *J. Chem. Crystallogr.*, vol. 40, pp. 201–206, 2010.

[96] X. Zhou, H. P. Zhang, G. Y. Wang, Z. G. Yao, Y. R. Tang, and S. S. Zheng, "Zeolitic imidazolate framework as efficient heterogeneous catalyst for the synthesis of ethyl methyl carbonate," *J. Mol. Catal. A Chem.*, vol. 366, pp. 43–47, 2013.

[97] Z.-X. Low, J. Yao, Q. Liu, M. He, Z. Wang, A. K. Suresh, J. Bellare, and H. Wang, "Crystal Transformation in Zeolitic-Imidazolate Framework," *Cryst. Growth Des.*, vol. 14, no. 12, pp. 6589–6598, 2014.

[98] W. Wu, J. Xie, and D. Xie, "Two Copper Complexes with Imidazole Ligands: Syntheses, Crystal Structures and Fluorescence," *Russ. J. Inorg. Chem.*, vol. 55, no. 3, pp. 384–389, 2010.

[99] W. J. Eilbeck, F. Holmes, and A. E. Underhill, "Cobalt(II), Nickel(II), and Copper(II) Complexes of Imidazole and Thiazole," *J. Chem. Soc. A*, pp. 757–761, 1967.

[100] G. Majano and J. Pérez-Ramírez, "Room temperature synthesis and size control of HKUST-1," *Helv. Chim. Acta*, vol. 95, pp. 2278–2286, 2012.

[101] J. Liu, L. Chen, H. Cui, J. Zhang, L. Zhang, and C.-Y. Su, "Applications of metal-organic frameworks in heterogeneous supramolecular catalysis." *Chem. Soc. Rev.*, pp. 6011–6061, 2014.

[102] O. Karagiaridi, M. B. Lalonde, W. Bury, A. A. Sarjeant, O. K. Farha, and J. T. Hupp, "Opening ZIF-8: a catalytically active zeolitic imidazolate framework of sodalite topology with unsubstituted linkers." *J. Am. Chem. Soc.*, vol. 134, no. 45, pp. 18 790–6, 2012.

# Appendix

Table A.1: FTIR band assignment for the spectral features of ZIF-8 and additional features present in the spectra shown in Figure 4.3 and Figure 4.11.

| **Wavenumber ($cm^{-1}$)** | **Vibration** |
|---|---|
| 695 | C−H bending |
| 760 | C−H bending |
| 994 | =C−H in plane bend |
| 1090 | =C−H in plane deformation vibration |
| 1145 | =C−H in plane deformation vibration |
| 1180 | =C−H in plane deformation vibration |
| 1310 | $CH_2$ wagging |
| 1382 | $CH_3$ asymmetric bend |
| 1423 | $CH_2$ asymmetric bend |
| 1451 | C=C stretch |
| 1584 | C=N stretch |
| 1979 | C=C asymmetric stretch |
| 2162 | C−H symmetric stretch |
| 2931 | C−H symmetric stretch |
| 3136 | =C−H stretch |
| | |
| 1679 | C=O stretch (DMF) |
| 1256 | N−$CH_3$ stretch (DMF) |
| 1063 | C−H bend (DMF) |
| 658 | N−C=O bend (DMF) |
| 1604 | C−O ($Mn(acac)_2$) |
| 1018 | $CH_3$ ($Mn(acac)_2$) |
| 919 | $CH_3$ ($Mn(acac)_2$) |

Figure A.1: Some manganese rates obtained by the exchange reactions of ZIF-8 with manganese (measured with AAS).

| Sample | Solvent used for ZIF-8 synthesis | Exchange time | Temperature | Zn loading (mmol/g) | Mn loading (mmol/g) | Mol% Mn |
|---|---|---|---|---|---|---|
| Mn 1 18.12.13 | MeOH | 24h (+2weeks) | 55℃ (+RT) | 4.58 | 0.73 | 13.7 |
| Mn 1+2 18.12.13 | MeOH | 24h (+2weeks) | 55℃ (+RT) | 3.82 | 3.84 | 50.1 |
| Mn 1.RT 02.04.14 | MeOH | 2 weeks | RT | 3.49 | 1.06 | 23.4 |
| Mn 2.RT 09.05.14 | MeOH | 2 weeks | RT | 4.13 | 0.61 | 12.8 |
| Mn 1 15.05.14 | Ammonia | 24h | 55℃ | 4.31 | 0.07 | 1.5 |
| Mn 2 15.05.14 | Ammonia | 24h | 55℃ | 4.00 | 0.05 | 1.3 |
| Mn 1 27.05.14 | MeOH | 24h | 55℃ | 5.35 | 0.19 | 3.5 |
| Mn 3 27.05.14 | MeOH | 24h | 55℃ | 3.86 | 0.59 | 13.3 |
| Mn 1_3 18.07.14 | MeOH | 72h | 55℃ | 3.62 | 0.81 | 18.3 |
| Mn 2_3 22.08.14 | MeOH | 72h | 55℃ | 4.59 | 0.70 | 13.2 |
| Mn 1.6 29.08.14 | MeOH | 6 days | 55℃ | 3.83 | 1.83 | 32.3 |
| Mn 2.6 19.09.14 | MeOH | 6 days | 55℃ | 2.61 | 3.14 | 54.5 |

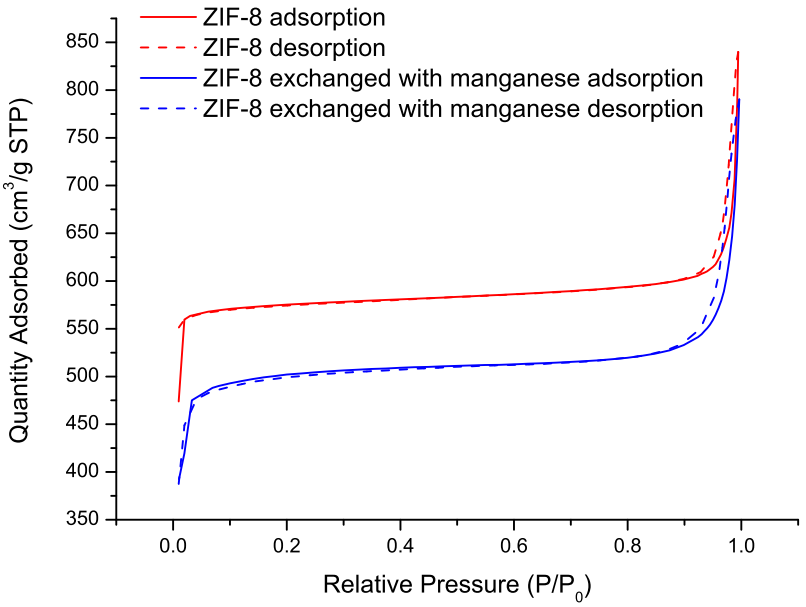


Figure A.2: $N_2$-physisorption isotherms for pure ZIF-8 and ZIF-8 exchanged with manganese. A decrease in the adsorbed amount of $N_2$ per gram material is shown for the manganese exchanged ZIF-8 compared to the pure ZIF-8.

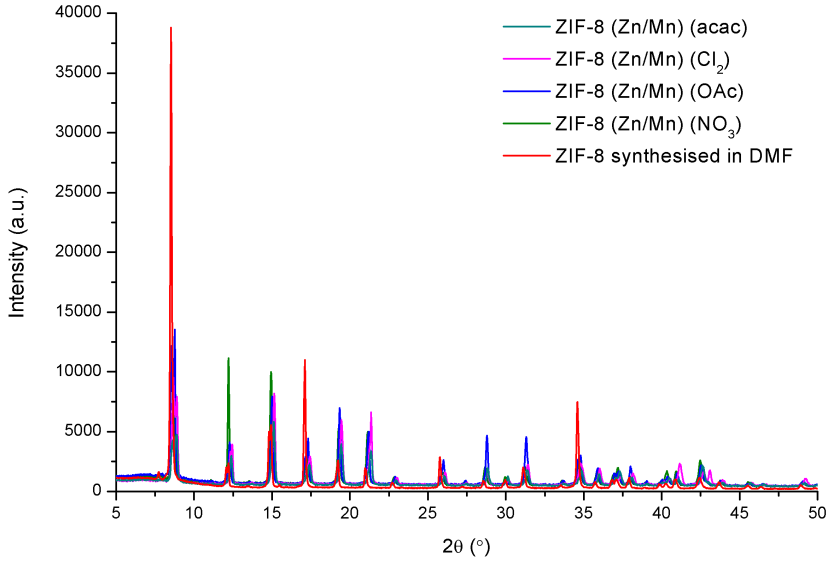


Figure A.3: X-ray diffractograms ZIF-8(Zn/Mn) synthesised directly using different precursors and pure ZIF-8 synthesised in DMF shown with their measured intensity. The same peak patterns are observed for all products, indicating that they all have the ZIF-8 structure. However, the peak intensities of the direct synthesised ZIF-8(Zn/Mn) is much lower than the intensity of the peaks of pure ZIF-8, indicating a lower crystallinity for the direct synthesised products.

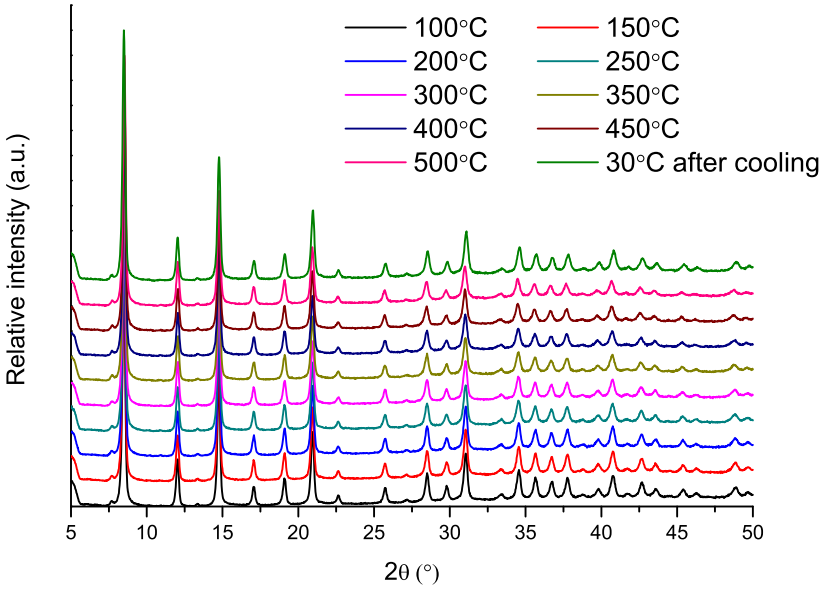


Figure A.4: X-ray diffractograms measured of ZIF-8 exchanged with manganese at different temperatures. No change in crystallinity was observed upon heating and after cooling.

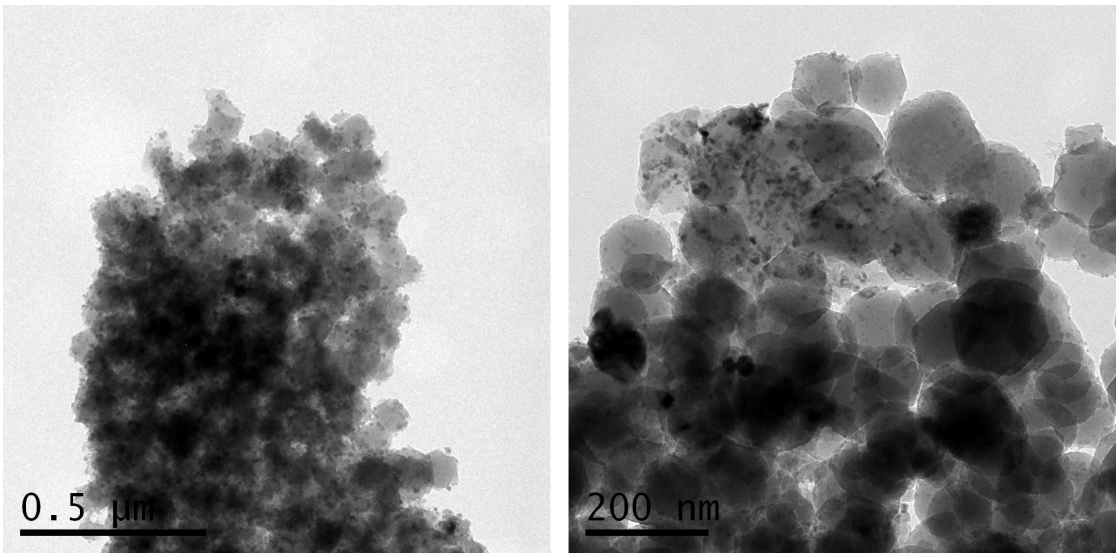


Figure A.5: TEM images of ZIF-8 after exchange with manganese (18 & 27% respectively found with AAS).

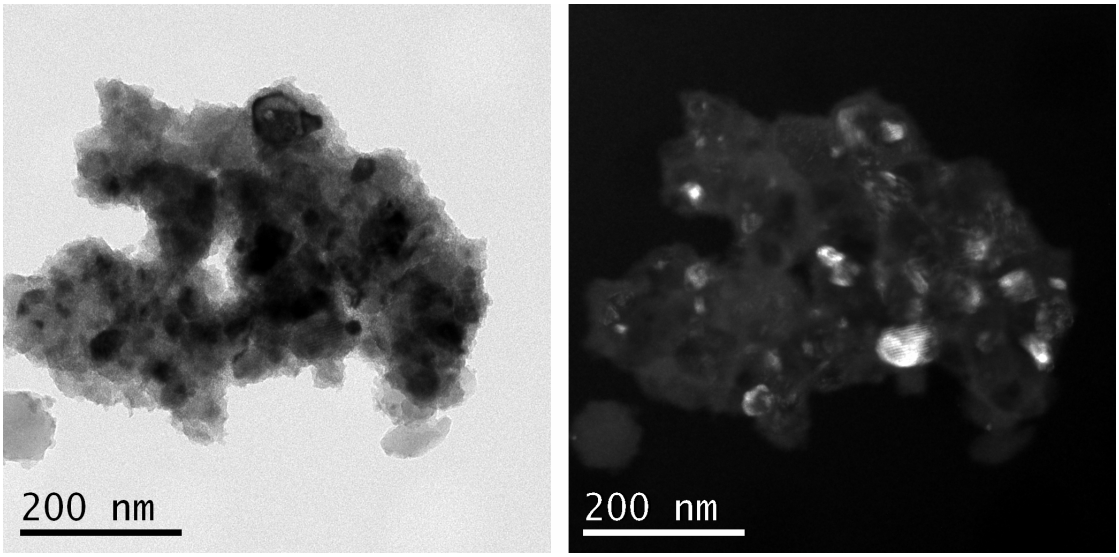


Figure A.6: Bright field TEM and HAADF-TEM of ZIF-8 exchanged with manganese (27% according to AAS).

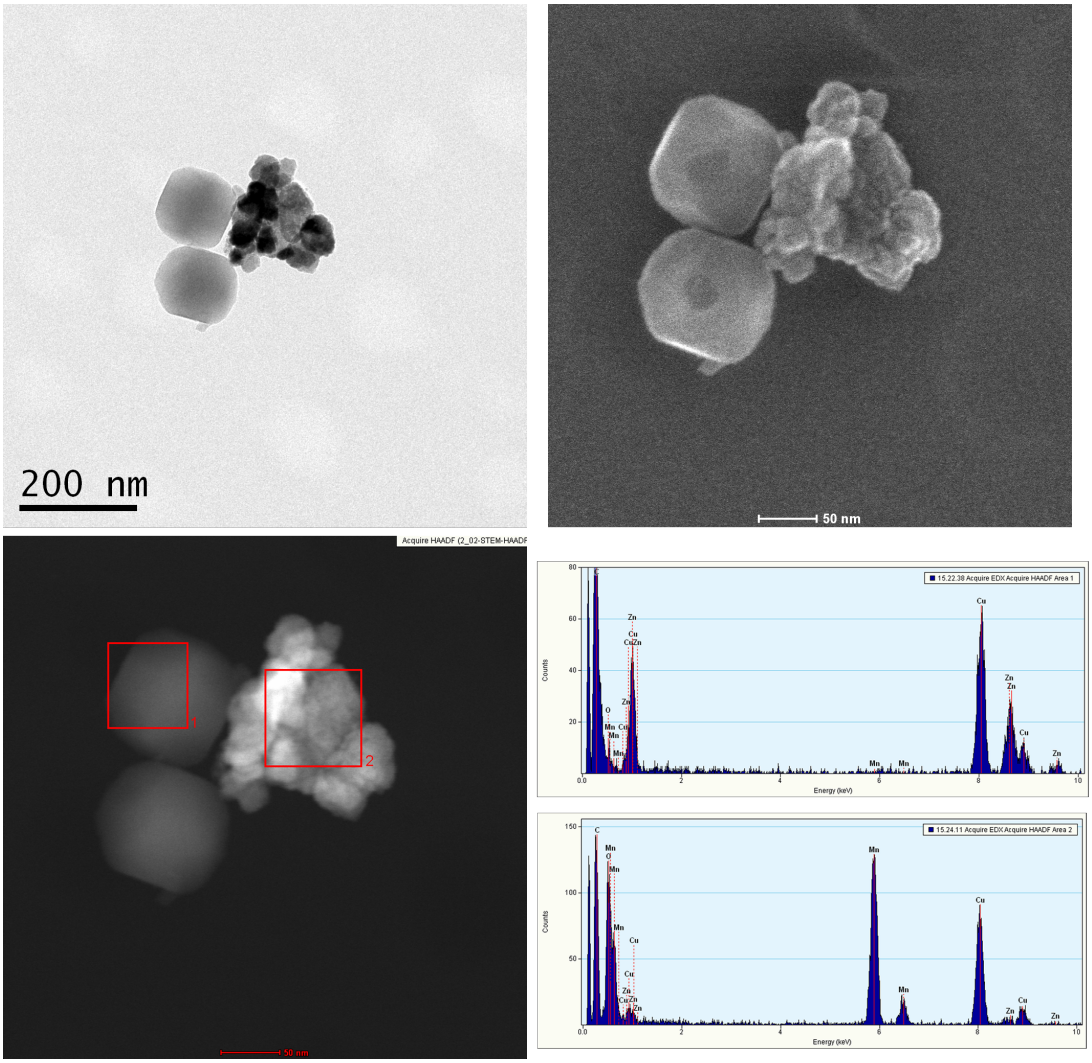


Figure A.7: TEM image of ZIF-8 exchanged with manganese (13% according to AAS). EDX measurements are shown, in area 1 the only metal present is zinc, in area 2 the only metal present is manganese.